J. Fluid Mech. (2004), *vol.* 514, *pp.* 281–312.
DOI: 10.1017/S0022112004000382 Printed in the United Kingdom

Sonic-boom noise penetration under a wavy ocean: theory

By H. K. CHENG AND C. J. LEE†

Aerospace and Mechanical Engineering, University of Southern California, Los Angeles, CA 90089-1191 USA

(Received 28 June 2002 and in revised form 26 April 2004)

Sonic-boom noise penetrating under a deep ocean is affected by its time-dependent interaction with the surface waves, which can significantly influence the perceived sound pressure level and tonal content of the disturbances at depth far greater than expected from the flat-ocean (Sawyers) model. The present theory assumes a small surface slope and a high water-to-air density ratio; the ocean surface in the analysis is modelled by a sinusoidal surface-wave train. The analysis shows that a distinct acoustic wave mode in the form of a packet of wavelets emerges in the sound field far below the surface and attenuates with increasing distance in a manner similar to the cylindrical spreading of monochromatic waves. The latter feature renders the surface waviness influence an effect of first-order importance, overwhelming the primary noise field at large depth. Detailed properties of the deep-water wave fields are examined and illustrated for the case of an incident N-wave, for which an explicit, analytic solution is obtained. The result reveals a similarity structure of the wave field with two distinct time scales and the invariance characteristics of the cylindrically spreading waves, in accord with the group-velocity concept of dispersive waves. An example is given of the interaction, illustrating the underwater waveform, sound-pressure and frequency levels.

1. Introduction

Issues of the potential impact of sonic booms on marine widelife were raised recently for sonic booms generated during military-aircraft and space-launch operations. Most studies of sonic-boom noise underwater have been based on Sawyers's (1968) model which stipulated a flat air–water interface. Cook (1970) elucidated Sawyers's model in more detail and Water (1971) confirmed certain qualitative features of Sawyers's theory in an experiment with an explosion over water. A more thorough simulation experiment on the sonic-boom noise penetration into water was undertaken by Intrieri & Malcolm (1973) in a ballistic range; the attenuation rate of the maximum overpressure with depth was found to be in agreement with Sawyers's prediction for an incident N-wave. Extensive applications of the model have been made to study the effects of aircraft flight Mach number and sonic-boom waveform by Sparrow (1995) and Sparrow & Ferguson (1997). These analyses found the noise penetration depth to be rather limited and the effects unimportant, except near the surface.

† Present Address: Appl. Sci. Lab., Inc. 2211 S. Hacienda Blvd., Suite 205, Hacienda Height, CA 91745, USA.

The present study finds, however, that a time-dependent effect arising from the interaction of an incident sonic boom with a wavy interface, though a secondary effect near the surface, can significantly alter the perceived sound-pressure level as well as the tonal content predicted at depth by the flat-ocean model. The effect in question is central to issues on the audibility and its impact in the short and long term. An important consideration omitted from the aforementioned works is the presence of the sea floor in shallow coastal water, on which the disturbances not only are expected to intensify but may excite sediment waves of comparable or greater amplitudes (Desharnais & Chapman 1998; Cheng, Kunc & Edwards 2003).

Undersea measurements of a sonic-boom wave field have recently been made by Sohn *et al.* (1999); the experiment involved planned supersonic overflights and shipboard pressure measurements. The waveform data agree well with Sawyers's prediction at 30–40 m below the surface, corresponding to one and a half times the sea-level signature length. Large discrepancies with Sawyers's prediction appear, however, at depths of 50 m and beyond. Apart from the high ambient noise level, inadequacy in the instrumentation and in the analysis procedures are evident from data recorded and examined at a depth of 50–75 m. Sohn *et al.*'s field measurements cannot be used, therefore, to assess the surface-wave influence in question. Moreover, the flight Mach numbers, reported to be less than 1.25, were too low to allow the wavy-surface effect to be detectable; this will be made apparent later (cf. § 5.4, and figure 3).

In this paper we study principally the theory of the (time-dependent) interaction problem and provide a solution with which the surface-wave influence can be more explicitly brought out. Examples of applications pertaining to the parameter ranges of practical interest are studied in Cheng, Lee & Edwards (2001), in which a quantitative basis for assessing the effect in question is established; the particular problems of rocket plumes, sea-floor presence and other effects are also examined therein. Similar results in this study have been presented in preliminary forms in Cheng & Lee (1998). As well as clarifying several observations in the original works and bringing out several new features, the following analysis will provide a solution which satisfies the radiation condition, which was not fully accounted for in the previous works. A more thorough description and discussion of some parts of the analysis are documented in the report version of this work (Cheng & Lee 2000). A laboratory study of the wavy-surface interaction effect has recently been presented in Fincham & Maxworthy (2001); the experimental measurements substantiate the principal results of our theory.

2. Preliminary remarks

The interaction model

The acoustic model considered consists of two interacting compressible, inviscid media, representing air and water. The formulation will assume an extremely large water-to-air density ratio ($\rho_W/\rho_A \gg 1$) and a water-to-air sound-speed ratio greater than unity ($a_W/a_A > 1$). As in all work on sonic booms, the overpressure $p' = p - p_A$ is small compared to the ambient atmosphere pressure p_A (i.e. $\epsilon = \max|p'/p_A| \ll 1$). The maximum surface slope departure from the horizontal, $2\pi\delta$, will be assumed to be small but much larger than the product of ϵ and the reciprocal of (ρ_W/ρ_A) (i.e. $\epsilon(\rho_A/\rho_W) \ll \delta \ll 1$). The analysis addresses the problem of a sinusoidal surface-wave train interacting with the sonic-boom wave. The wave field reaching the interface

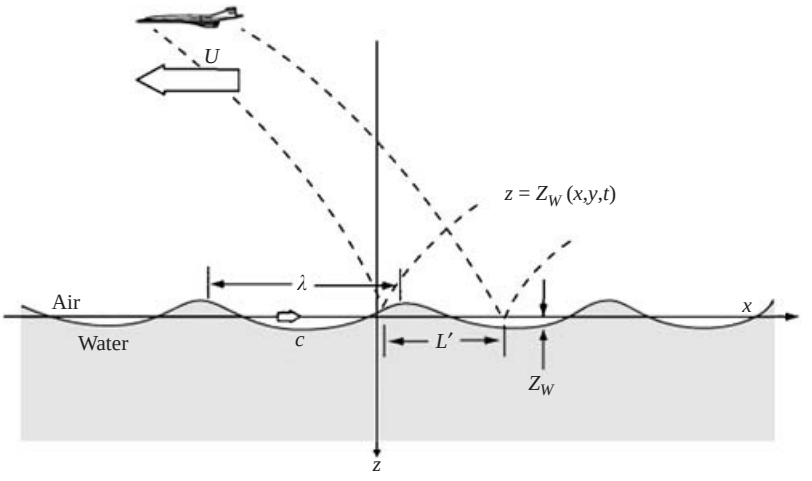

FIGURE 1. Sketch illustrating the air–water interface, coordinates, and notation.

will be assumed to propagate with a uniform (or nearly uniform) horizontal velocity component U (in the negative x-direction observed from a rest frame, cf. figure 1).

One feature that greatly simplifies the modelling of the interaction problem in three spatial dimensions is the extremely small dimension of the sonic-boom impact zone in the flight direction compared to its transverse horizontal scale, as depicted by the sketch in figure 2. This is evident from overpressure contours at sea level determined in sonic boom analyses (Hayes 1971; Carlson & Maglieri 1972) where the aspect ratio of the impact zones is as high as 200–500. The problem formulation in this case may therefore follow the lifting-line approach (as described in Van Dyke 1975) which reduces the leading-order problem to a two-dimensional one. Thus, in addition to $\epsilon(\rho_A/\rho_W) \ll \delta \ll 1$, the reciprocal of the aspect ratio, $(AR)^{-1}$, will also be regarded as being much smaller than the surface slope parameter δ. There is no other restriction on the relative magnitudes of ϵ and (ρ_A/ρ_W) with respect to δ, so long as they remain small compared to unity, as will be explained later.

Anticipated features

The analysis will focus primarily on the reduced two-dimensional problem in which the wave field underwater is subsonic in that the horizontal (vehicle/wave field) speed U is less than the water sound speed, i.e. $M_W \equiv U/a_W < 1$. Under standard conditions, this means that the Mach number in the air $M_A \equiv U/a_A$ remains below $a_W/a_A = 4.53$. The disturbances in this subsonic wave field are expected to attenuate with increasing depth z. Under a flat ocean, the overpressure from a sonic boom would attenuate rapidly with depth as z^{-2} in most cases (Sawyers 1968; Sparrow 1995). Under a wavy ocean, however, the dominant wave mode produced by the interaction will appear at large depth in the form of a packet of wavelets; the overpressure of each wavelet attenuates at a much lower rate as $1/\sqrt{z}$, in accord with the cylindrical-spreading rule of monocromatic waves from a line source (see e.g. Landau & Liftshitz 1959). These overwhelm the otherwise primary flat-ocean wave field by virtue of their much slower attenuation rate. These and other properties reflect the dispersive character of a deep-water wave field, as will be delineated and made more specific by the following analysis. A rough water surface is also known to augment sound transmission from air to water, as has been indicated by analyses (Medwin, Helbig &

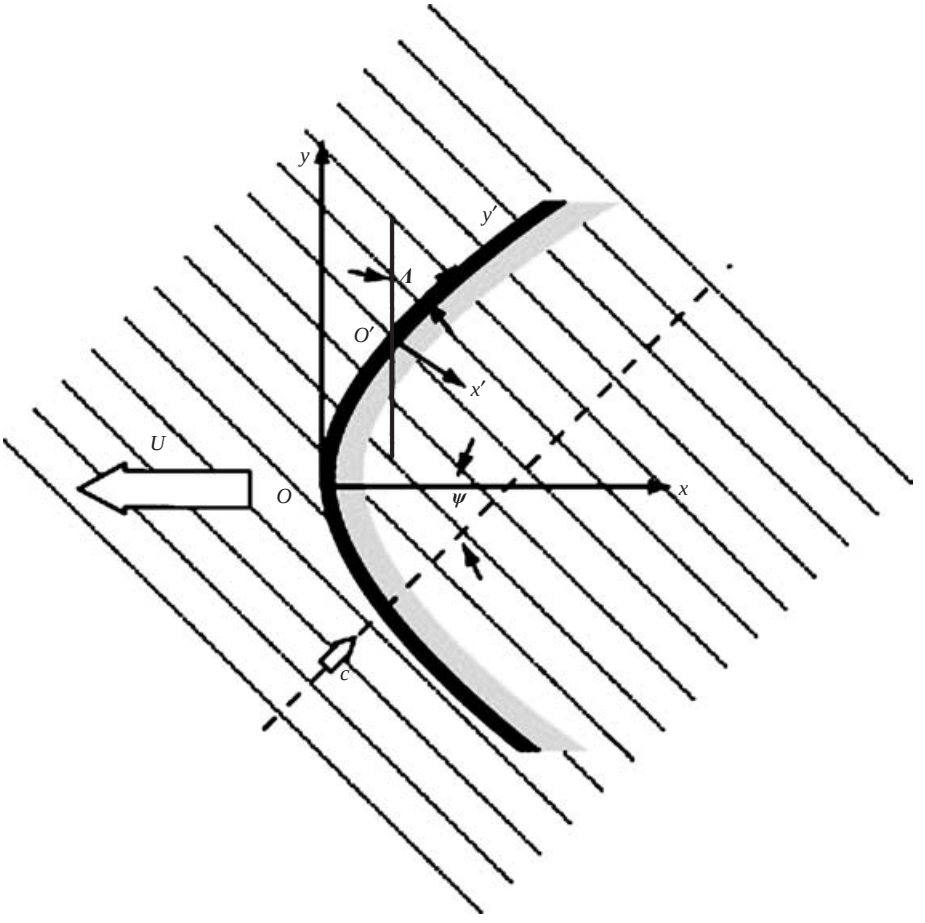

FIGURE 2. Sketch illustrating coordinate systems and notation in the analysis of the interaction of a sonic-boom wave and surface-wave train.

Hagy 1973), with supporting experimental evidence. This apparent consistency with our analysis, however, cannot be taken as direct support of the present theory, since, unlike the problem at hand, their study stipulated a wavelength small compared to the signature/pulse length, as well as an unlimited time duration for observing the rough-sea statistics. The present analysis may nevertheless be regarded as an extension of Medwin *et al.*'s (1973) study.

The condition $M_A < 4.53$ for a subsonic underwater wave field corresponds to the incident ray angle $\theta_i > \sin^{-1}(a_A/a_W) \approx 12.75^\circ$ associated with the 'total reflection' phenomenon in ray acoustics theory (see for example, Tolstoy 1987; Pierce 1991). The prohibition of acoustic energy transmission under this condition would have ruled out the existence of a (subsonic) underwater wave field. Recall however that the ray approximation is inapplicable at a depth comparable to the underwater signature length, where the crucial input to the deep-water wave field is generated. In the case of a supersonic wave field occurring underwater, i.e. $M_W \equiv U/a_W > 1$ and $M_A \equiv U/a_A > 4.53$, the two-dimensional wave field under a flat ocean would lead to an uninhibited propagation until three-dimensional effects take over at some large depth.

Nonlinear, numerical computation

The problem of a sonic-boom wave interacting with a truncated surface-wave train was studied numerically by Rochat & Sparrow (1997), employing a finite-difference procedure capable of capturing contact discontinuities. Solutions were obtained for examples with small wave heights corresponding to $\delta \ll 1$; however results were presented only at a depth very small compared to the signature length, where the overpressure obtained reveals mainly the small, secondary effect, as anticipated.

Underwater audibility

Experiments on sonic-boom effects on marine wildlife (Bowles 1995; Bowles & Stewart 1980) have raised concerns about the sound levels (and rise time) that may cause a temporary shift in the hearing threshold of pinnipeds and other mammals living on or near the shore. That the sonic boom noise can be perceived/discerned by marine mammals under water is similar to concerns about vessel and (undersea) air-gun noise (Richardson *et al.* 1995; Greene 1995) and the effects of low-frequency active and passive sonars (see Munk, Worchester & Wunsch 1995; Au 1997; Frankel & Clark 1998). Of particular interest in this regard are the documented sound levels and dominant frequency ranges of whale calls (see Richardson *et al.* 1995); whether sonic-boom disturbances can be distinguished from the undersea ambient noise in these sound-pressure and frequency ranges is another issue that the present analysis may help to address.

3. The interaction model and reduced equations

3.1. *The assumption of high water-to-air density ratio*

Basic to the present study is the assumption of an interface separating two inviscid compressible media, across which the pressure and normal velocity, in the absence of surface tension, are continuous. As pointed out earlier, the water-to-air density ratio ρ_W/ρ_A will be assumed to be much greater than unity. This ratio, being 773.4 under standard conditions, causes the ocean to behave very stiffly in its response to an incident sonic-boom wave, with vanishingly small changes in the underwater fluid velocity $\boldsymbol{u}'$ and in the interface geometry. The study will employ two sets of Cartesian coordinates in which the positive z-axis points from the air to water, as indicated in figure 1.

A Cartesian frame fixed to the fluid in a rest state will be used in the formulation in §§3.2, 3.3, whereas the analysis in §3.4 and the subsequent analysis employ a frame moving with the sound source at speed U (relative to the rest frame). Pressure changes are taken to be the difference from the equilibrium value $p_\infty + \rho g z$, although the $\rho g z$ contribution in the domain above the water of $|z| = O(L')$ is negligible. The analysis will consider a surface-wave train over deep water with a small surface slope of order δ and wave speed $|c| \ll U$. The wind speed near the surface is also assumed to be small, being not much greater than $|c|$; this condition appears to be applicable to the fully developed sea and swell (Bascom 1964). Whereas ϵ, δ, c, $(AR)^{-1}$ and (ρ_A/ρ_W) must all be small compared to unity, the main parametric requirement on their relative magnitudes is only

$$(AR)^{-2}, \epsilon(\rho_A/\rho_W) \ll \delta, c/U.$$

This is to ensure that the time-dependent interaction corrections are the most dominant among the secondary effects under water (at all depth levels) and is explained at the end of §3.3.

3.2. *A priori estimates*

The extremely stiff behaviour of the water in response to the sonic boom may be more explicitly delineated with the help of *a priori* estimates. Subscript symbols A for air and W for water will be applied to the pressure p, density ρ, sound speed a and velocity (vector) $\boldsymbol{u}$. The equation describing the interface in a rectilinear Cartesian frame is

$$z = Z_W(x, y, t). \tag{3.1}$$

This surface has a characteristic slope of order δ ($2\pi\delta$, more precisely), an x-length scale λ, and a t-time scale λ/c. We shall denote the departure from the equilibrium state in the absence of the sonic boom by a superscript $^\circ$; a prime is used to denote the additional departure due to the sonic boom. Utilizing the continuity requirement for pressure and normal velocity across the interface, and the approximate estimate $|p'| \sim \rho a |\boldsymbol{u}'|$, together with the Bernoulli relation, one arrives at a set of order-of-magnitude estimates for the underwater acoustic-field variables

$$p'_W = O(p'_A) = O(\epsilon \rho_A U^2), \tag{3.2a}$$

$$\left|\frac{u'}{U}\right|_W, \quad \left(\frac{a_A}{a_W}\right)^2 \left|\frac{\rho'}{\rho}\right|_W, \quad \frac{1}{U}(Z'_W)_t = O\left[\left(\epsilon \frac{\rho_A}{\rho_W}\right)\right]. \tag{3.2b}$$

These parametric estimates are confirmed by the internal consistency of the subsequent analysis. In the absence of the sonic boom, the perturbation quantities from the equilibrium state underwater are estimated to be

$$p^\circ_W = O(\delta \rho_W c^2), \tag{3.3a}$$

$$\left|\frac{\boldsymbol{u}^\circ}{c}\right|_W, \quad \left(\frac{a}{c}\right)^2_W \left|\frac{\rho^\circ - \rho_\infty}{\rho}\right|_W, \quad \frac{1}{c}\left|\left(Z^\circ_W\right)_t\right| = O(\delta), \tag{3.3b}$$

where ρ_∞ is the upstream density taken as a reference quantity. The estimates of the orders of p' and $\boldsymbol{u}'$ in (3.2) assume a spatial scale of L' (the signature length) and a time scale of L'/U, whereas the estimates for p° and $\boldsymbol{u}^\circ$ in (3.3) are based on the spatial scale λ and time scale λ/c.

3.3. *Key equations; decoupling the interaction effect*

For the inviscid problem at hand, the assumption of existence of a velocity potential for each medium will suffice. With the orders established for ρ° and ρ' from (3.2), (3.3), the compressibility correction to the mass conservation equation, namely,

$$\frac{1}{\rho}\frac{\mathrm{D}}{\mathrm{D}t}\rho,$$

can be linearized; thereby the continuity equation in the underwater rest frame can be reduced to one governing the velocity potentials and the overpressure underwater

$$\left[a_W^2 \nabla^2 - \frac{\partial^2}{\partial t^2}\right]\begin{pmatrix}\phi^\circ + \phi' \\ p^\circ + p'\end{pmatrix} = 0 \tag{3.4}$$

with terms omitted of a higher order

$$\left[\delta^2\left(\frac{c}{a}\right)^2 + \epsilon\frac{\rho_A}{\rho_W}\right]\left(\frac{a_A}{a_W}\right)^2.$$

The product $\epsilon(\rho_A/\rho_W)$ in the square brackets arises from remainders accounting for the fluid compressibility. The same equation with a_W and ρ_W replaced by a_A and ρ_A

holds above water. Owing to the limited vertical length scale considered, effects of stratification in ρ and a as well as the full nonlinear effect have not been included.

Successive applications of the interface boundary conditions will permit an unambiguous determination of the interaction effect on the interface geometry, Z'_W, although the latter is too small to be of practical significance. In Cartesian coordinates fixed to the rest frame, this condition for the normal fluid velocity on each side of the interface $z = Z_W(x, y, t)$ may be expressed as

$$w^\circ + w' = \left(\frac{\partial}{\partial t} + u^\circ\frac{\partial}{\partial x} + v^\circ\frac{\partial}{\partial y}\right) Z^\circ_W + \left(u'\frac{\partial}{\partial x} + v'\frac{\partial}{\partial y}\right) Z^\circ_W + \left[\frac{\partial}{\partial t} + u^\circ\frac{\partial}{\partial x} + v^\circ\frac{\partial}{\partial y}\right] Z'_W + \left[u'\frac{\partial}{\partial x} + v'\frac{\partial}{\partial y}\right] Z'_W \quad (3.5)$$

where $\boldsymbol{u}^\circ = \nabla\phi^\circ$ and $\boldsymbol{u}' = \nabla\phi'$. Accordingly, ϕ° can be decoupled from ϕ' and solved with the first line of (3.5) (dropping w' on the left) as boundary conditions. By virtue of the magnitude estimates for the wave field above water and those in (3.1)–(3.3) underwater, the leading approximation to w' is seen from (3.5) to be identically zero at the interface. Thereby Sawyers's (1968) model is recovered as a leading approximation to ϕ'. Namely, at $z = 0$, for the leading approximation,

$$\frac{\partial\phi'}{\partial z} = 0. \quad (3.6)$$

Applying (3.5) to the interaction problem above the water for the next approximation, terms with partial derivatives of Z'_W are seen to be smaller in magnitude than those with partial derivatives of Z°_W on the second line by order (ρ_A/ρ_W); therefore those with Z°_W can be used as a downwash correction to the flat-interface model in the wave reflection problem above water. The solution procedure for ϕ' and p' above and under the interface will be more explicitly described below.

From the PDE (3.4) and the boundary condition (3.5), the relative importance of the several second-order corrections to the underwater wave field may be assessed in terms of ϵ, δ, (ρ_A/ρ_W) and $(AR)^{-1}$. Those other than the time-dependent corrections of order $\epsilon\delta$ are expected to be comparable to δ^2 and terms proportional to ϵ^2. The δ^2 terms pertain to weak nonlinear corrections to ϕ° and p° (of order δ) in the absence of sonic booms, and their solutions can be decoupled from the wavy-surface interaction problem, as noted earlier. However, terms proportional to ϵ^2 are nonlinear corrections to the Sawyers non-wavy model for a flat ocean; they either enter as corrections from (standard) sonic-boom calculations above water which have already been included in the surface value of p° or ϕ°, or as the under-water compressibility correction in the PDE (3.4), as well as the correction to the water surface geometry under a sonic-boom overpressure through the boundary condition (3.5). With the order of magnitudes from § 3.2 given to ϕ^0, p^0, ϕ', p', Z^0_W and Z'_W in both equations, the magnitude of terms proportional to ϵ^2 is seen to be of order $\epsilon^2(\rho_A/\rho_W)$, which is much smaller than ϵ^2 itself. On the other hand, the time-dependent interaction effects in both these equations are seen to have order $\epsilon\delta$, while other higher-order corrections found are of order $\epsilon\delta(\rho_A/\rho_W)$, $\epsilon\delta(AR)^{-1}$, and $\epsilon(AR)^{-2}$. Therefore, with ϵ, (ρ_A/ρ_W), and $(AR)^{-1}$ being small compared to unity, the parametric requirement

$$\epsilon(\rho_A/\rho_W), (AR)^{-2} \ll \delta$$

stated earlier in § 3.1 ensures the dominance of the time-dependent interaction effect among the secondary corrections at all depth levels. Owing to the extremely small

air-to-water density ratio in this requirement, the analysis developed below is expected to remain applicable even for an ϵ significantly larger than the slope parameter δ, therefore allowing a great degree of freedom for laboratory study of the phenomenon of interest. The simplification of a small c/U will also be made in the analysis.

3.4. *The problems above and under the interface*

From the above discussion, the interaction problem for ϕ' above water may be solved in the leading and the next orders using the downwash w' in (3.5) on top of the interface as boundary conditions, a procedure in common with that for the analysis in supersonic aerodynamics (Miles 1959; Ashley & Landahl 1968). Underwater, one may solve for ϕ' or p' (which satisfies the same PDE) with the ϕ' or p' distribution furnished by the solution above water.

In the following, the Cartesian frame moving with velocity U will be employed. The incident wave system (from the air/space craft) in the vicinity of the interface is assumed to be independent of time in this frame. Let ϕ_1' and ϕ_2' represent solutions corresponding to the three-dimensional version of Sawyers's theory and that which accounts for the time-dependent surface interaction effect, respectively. The PDEs and boundary conditions at $z=0$ for ϕ_1' and ϕ_2' above water are, respectively

$$\left[(1-M^2)\frac{\partial^2}{\partial x^2}+\left(\frac{\partial^2}{\partial y^2}+\frac{\partial^2}{\partial z^2}\right)\right]\phi_1'=0, \tag{3.7a}$$

$$\frac{\partial \phi_1'}{\partial z}=0 \quad \text{at } z=0; \tag{3.7b}$$

and

$$\left[(1-M^2)\frac{\partial^2}{\partial x^2}+\left(\frac{\partial^2}{\partial y^2}+\frac{\partial^2}{\partial z^2}\right)-2\frac{U}{a^2}\frac{\partial^2}{\partial x\,\partial t}-\frac{1}{a^2}\frac{\partial^2}{\partial t^2}\right]\phi_2'=0, \tag{3.8a}$$

$$\frac{\partial \phi_2'}{\partial z}=\left[\left(\frac{\partial}{\partial x}\phi_1'\right)\frac{\partial}{\partial x}+\left(\frac{\partial}{\partial y}\phi_1'\right)\frac{\partial}{\partial y}\right]Z_W^\circ-\left(\frac{\partial^2\phi_1'}{\partial z^2}\right)Z_W^\circ, \text{ at } z=0, \tag{3.8b}$$

where the last term in (3.8*b*) results from transferring the interface boundary condition to the plane $z=0$. The subscript A has been dropped from ϕ_1' and ϕ_2', and also from a and $M\equiv U/a$, for convenience. The M in (3.7*a*, *b*) is greater than unity for the supersonic wave field above the water considered. The need for the prescription of (upstream) incident wave data for ϕ_1', and the allowance for the (reflected) outgoing waves in ϕ_2', are understood.

Under water, the PDEs for the ϕ_1' and ϕ_2' and the corresponding overpressure p_1' and p_2' remain in the form (3.7), (3.8), except that $M<1$ and $a=a_W>a_A$. The subsonic underwater wave field of p_1' and p_2' will be solved as problems with boundary values prescribed by the surface pressure above water at $z=Z_w^\circ$ transferred to the reference plane $z=0$:

$$p_1'=-\left(\rho U\frac{\partial}{\partial x}\phi_1'\right)_A, \tag{3.9a}$$

$$p_2'=-\left[\rho\left(\frac{\partial}{\partial t}+U\frac{\partial}{\partial x}\right)\phi_2'\right]_A-\left(\frac{\partial p_1'}{\partial z}\right)_W Z_W^\circ. \tag{3.9b}$$

Local breakdown of the approximation may occur where $\partial p_1'/\partial z$ in (3.9*b*) becomes unbounded, as at $x=0, 1$ for an N-wave. This breakdown does not affect the solution

validity elsewhere, as shown in the discussion after § 5.3 below. The wind effect on p' could also be accounted for through ϕ', in (3.9*a*), by readjusting the value of M in (3.7*a*). This adjustment is unnecessary in practice, since incident wave data from either sonic-boom computer codes or field measurements must have included the effect in question. For the present problem with $M_W < 1$ in the absence of a sea floor, both p_1' and p_2' underwater are required to vanish with increasing z.

4. Sawyers's theory as leading approximation

Sawyers's (1968) analysis for a flat ocean pertains to a two-dimensional subsonic wave field in the absence of a sea floor. The resulting wave-field similitude corresponds to the Prandtl–Glauert rule in aerodynamics and has been applied to assessing effects of flight Mach number and waveform by Sparrow (1995) and Sparrow & Ferguson (1997). The result may be expressed more comprehensively as a complex Hilbert integral

$$p' = \mathrm{Im}\frac{1}{\pi}\int_{-\infty}^{\infty}\frac{p'(x_1,0)\,\mathrm{d}x_1}{x_1-\zeta} \tag{4.1a}$$

where ζ is the complex variable embodying the subsonic Prandtl–Glauert similitude

$$\zeta \equiv \frac{x}{L'} + \mathrm{i}\beta\frac{z}{L'}, \qquad \beta \equiv \sqrt{1-M_W^2} \tag{4.1b, c}$$

and Im denotes for the imaginary part. This elliptic underwater field cannot support shock discontinuities, resolving rapidly (with distance) any spike-like waveform prescribed at the interface. For an incident N-wave

$$\frac{p'(x,0)}{p'_{max}} = 1-2x, \qquad 0<x<1$$
$$= 0, \qquad x<0, x>1,$$

the result can be more explicitly expressed as

$$\tilde{p}' = \frac{p'}{p'_{max}} \equiv \frac{1-2x}{\pi}\left[\tan^{-1}\left(\frac{x}{\beta z}\right) - \tan^{-1}\left(\frac{x-1}{\beta z}\right)\right] - \frac{1}{\pi}\ln\left|\frac{(x-1)^2+\beta^2z^2}{x^2+\beta^2z^2}\right|. \tag{4.1d}$$

Essential to subsequent discussions is this field's behaviour at large distance ($|\zeta| \gg 1$)

$$p' \sim -\mathrm{Im}\frac{1}{\pi}\int_{-\infty}^{\infty} p'(x_1,0)\,\mathrm{d}x_1/\zeta + \mathrm{Im}\frac{1}{\pi}\int_{-\infty}^{\infty} x_1 p'(x_1,0)\,\mathrm{d}x_1/\zeta^2. \tag{4.2}$$

The second term signifies a (dipole-like) z^{-2} attenuation rate, to be expected in most applications since the integral representing the total sonic-boom impulse in the first term vanishes for most aircraft applications. Cases with a non-vanishing impulse cannot be ruled out; examples from rocket space-launch applications show that the integral values are negative and therefore p' has a sink-like z^{-1} behaviour (Cheng *et al.* 2001). In the following development for the three-dimensional problems with a high AR, these descriptions provide the leading approximation to the overpressure in a plane normal to the centreline of the surface impact zone (cf. figure 2).

5. Surface-wave interaction effect

5.1. *Sinusoidal surface-wave train*

We consider a sinusoidal wave train on the interface. In the (rest) stationary frame $(\underline{x}, \underline{y}, \underline{z})$ fixed to the ocean bottom, the surface elevation is given by

$$Z_W^\circ = \delta\lambda e^{i[(k_1\underline{x}+k_2\underline{y})-\omega t]}. \tag{5.1}$$

In the steadily moving coordinates used in (3.7), (3.8), this surface will be given by (cf. figure 1)

$$Z_W^\circ = \delta\lambda\, e^{i[k_1 x+k_2 y-\Omega t]} \tag{5.2a}$$

where the frequency Ω depends on the surface wavenumber and the relative horizontal velocity through

$$\Omega = ck + Uk_1 = k(c + U\cos\psi). \tag{5.2b}$$

Note that $k=(k_1^2+k_2^2)^{1/2}$, $ck=\omega$, and c is the phase velocity of the surface wave in the rest-frame $(\underline{x}, \underline{y}, \underline{z})$, and that $\cos\psi$ is the directional cosine of the wavenumber vector of the surface-wave train with respect to the x-axis along the flight track (opposite to the flight direction; cf. figures 1, 2). Since $|\psi| \leqslant \pi/2$ (cf. figure 2), k_1 and Ω are positive. More general results can be built up from the solution for (5.2) as Fourier series/integral. The surface wave velocity c is small compared to U or a, but may nevertheless be retained in the formulation to allow passage to the limit $U/c \longrightarrow 0$. Henceforth, the real parts of $Z_W^\circ, \phi^\circ, \phi'$ and p' are to be understood. In view of the discussion in § 3.4, the three-dimensional interaction solution can be studied for a sonic-boom impact zone of very high aspect ratio, for which the reduced two-dimensional problem is solved in a plane normal to the centreline. A strictly two-dimensional version of the development was studied earlier in Cheng & Lee (1997). The relative magnitudes of $(AR)^{-1}, \epsilon$ and δ assumed here permit the application of (3.7)–(3.9) with x, y, z considered as local Cartesian coordinates.

5.2. *Supersonic wave field above water*

Leading approximation

We shall assume that the component wave field is supersonic, i.e. $M_n = M\cos\Lambda > 1$, where Λ is the *local* centreline sweep angle. In the local Cartesian frame, with the x'-axis normal to the leading edge of the impact zone, $x = x_{\mathrm{LE}}(y)$ as indicated by figure 1, the solution to (3.7) corresponding to the flat-ocean model yields

$$\phi_1' = f(x' - B_n z') + f(x' + B_n z') \tag{5.3}$$

where $B_n = (M^2\cos^2\Lambda - 1)^{1/2}$.

Next approximation

Among the corrections to the Sawyers solution ϕ_1' are those arising from the three-dimensional effect, the (media) nonlinear effect and the effect generated from the interaction of the sonic boom with the wavy ocean surface. The latter will be the focus of the present analysis for reasons noted earlier. The equation for the surface depression of the wave train in (5.2a) for $AR \gg 1$ is invariant with respect to a local coordinate rotation:

$$Z_W^\circ = \delta\lambda\, e^{i(k_1' x' + k_2' y') - i\Omega t}, \tag{5.4a}$$

since $k_1 x + k_2 y = k_1' x' + k_2' y'$, where k_1' is positive (cf. figure 2).

For future reference, we observe that

$$k_1' = k\cos(\Lambda + \psi),\ \ k_2' = k\sin(\Lambda + \psi) \tag{5.4b}$$

and that

$$k_1 = k_1'\cos\Lambda + k_2'\sin\Lambda, \qquad k_2 = -k_1'\sin\Lambda + k_2'\cos\Lambda. \tag{5.4c}$$

At $\Lambda = -\psi$ where, in the moving frame, the surface-wave train is seen to strike the section normally, $k_2' = 0$ and $k_1' = k$.

A solution to (3.8*a*) in a synchronous (mode) form

$$\phi_2' = \hat{\phi}_2\, \mathrm{e}^{\mathrm{i}k_2' y'}\, \mathrm{e}^{-\mathrm{i}\Omega t} \tag{5.5}$$

is anticipated for the sinusoidal surface-wave train (5.4*a*). The impermeability condition (3.8*b*) becomes one for $\hat{\phi}_2$ at $z = 0$:

$$\frac{\partial}{\partial z}\hat{\phi}_2 = 2\delta\lambda\, \mathrm{e}^{\mathrm{i}k_1' x}\left[\mathrm{i}k_1'\frac{\mathrm{d}}{\mathrm{d}x'} - B_n^2\frac{\mathrm{d}^2}{\mathrm{d}x'^2}\right] f(x'); \tag{5.6}$$

it furnishes an input to the wave field ϕ_2' above water synchronous with the oscillatory surface wave (5.4*a*). The equation (3.8*a*) governing ϕ_2' above water thereby reduces to a hyperbolic PDE for $\hat{\phi}_2$ in x' and z':

$$\left[(M_n^2 - 1)\frac{\partial^2}{\partial x'^2} - \frac{\partial^2}{\partial z'^2} - \mathrm{i}P\frac{\partial}{\partial x'} - Q\right]\hat{\phi}_2 = 0 \tag{5.7a}$$

with

$$M_n = U\cos\Lambda/a, \quad P \equiv 2\frac{\Omega M_n}{a} - 2k_2'\tan\Lambda M_n^2, \tag{5.7b, c}$$

$$Q \equiv \left(\frac{\Omega}{a} - k_2' M_n\tan\Lambda\right)^2 - (k_2')^2. \tag{5.7d}$$

Helpful to what follows are the expressions for P and Q simplified for a small c/U, which are more explicitly related to wavenumber k, the impact-zone (local) sweep angle Λ, and the relative surface-wave train angle ψ:

$$P = 2kM_n^2\cos(\Lambda + \psi), \tag{5.7e}$$

$$Q = \left(\frac{P}{2M_n}\right)^2 - (k_2')^2 = k^2\left[M_n^2 - \left(1 + M_n^2\right)\sin^2(\Lambda + \psi)\right]. \tag{5.7f}$$

Up to the present stage, k, P and Q have not been normalized and have the dimensions $(L')^{-1}$, $(L')^{-1}$ and $(L')^{-2}$, respectively.

Solution by Laplace transform

Solving for the $\hat{\phi}_2$ above water by Laplace transform satisfying (5.6), (5.7) yields a solution in a convolution integral form, involving the Bessel function of the first kind, order zero,

$$\hat{\phi}_2(x', z) = -2\frac{\delta\lambda}{B_n}\int_0^{x' + B_n z} \mathrm{e}^{\mathrm{i}k_1'(x' - x_1')}\left[\mathrm{i}k_1'\frac{\mathrm{d}}{\mathrm{d}x'} - B_n^2\frac{\mathrm{d}^2}{\mathrm{d}x'^2}\right] f(x' - x_1') \times \mathrm{e}^{\mathrm{i}(P/2B_n^2)x_1'} J_0\left(\alpha\sqrt{(x_1')^2 - B_n^2 z^2}\right)\mathrm{d}x_1' \tag{5.8a}$$

where $\mathrm{d}^2 f/\mathrm{d}x'^2$ results from the boundary-condition transfer in (3.8*b*) and is to be treated in the Stieltjes sense, and

$$\alpha \equiv \sqrt{P^2 - 4B_n^2 Q}\,/2B_n^2. \tag{5.8b}$$

The terms under the square root can be re-expressed as

$$P^2 - 4B_n^2 Q = 4\big(M_n^2 - 1\big)(k_2')^2 + 4\left(\frac{\Omega}{a} - k_2' M_n \tan\Lambda\right)^2; \tag{5.8c}$$

therefore α is real and positive as long as the normal Mach number M_n above water at the position is greater than unity. For a negligibly small c/U, (5.7e, f) are applicable and

$$\alpha = k\sqrt{M_n^2 - \sin^2(\Lambda + \psi)}/B_n^2. \tag{5.8d}$$

The correction to the surface overpressure above water at $z = 0$ (needed for solving the inverse problem under water) is, after simplification for small c/U,

$$p_2' = -\rho\frac{\mathrm{D}'}{\mathrm{D}t}\phi_2 = -\rho U_n \mathrm{Re}\left[\mathrm{e}^{\mathrm{i}k_2' y'}\,\mathrm{e}^{-\mathrm{i}\Omega t}\left(\frac{\mathrm{d}}{\mathrm{d}x'} - \mathrm{i}k_1'\right)\hat{\phi}_2(x', 0)\right], \tag{5.8e}$$

where Re denotes real part.

Evaluating $\hat{\phi}_2(x', 0)$ *for the* N-*wave*

For convenience, x and x', will be made dimensionless with L'; k and k' with $(L')^{-1}$; and f with $\epsilon U L'$. Correspondingly, Ω/a in (5.7c, d) is normalized by the reciprocal of (L'), as for k. Since the function $f'(\xi)$ admits shock discontinuities at $\xi = 0, 1$ and vanishes beyond $0 < \xi < 1$, the integral of (5.8a) will be evaluated separately for the range $0 < x_1 < 1$ and the range $1 < x_1 < \infty$. In the subsequent calculation for an incident N-wave, for which (cf. (5.3))

$$f'(\xi) = (2\xi - 1)1(\xi)1(1 - \xi), \tag{5.9}$$

where $1(\xi)$ stands for a unit-step function, the overpressure behind the (incident) front shock is $p' = \rho U_n^2 \epsilon$. The normalized surface value of $\hat{\phi}_2$ will be evaluated for $0 < x' < 1$ as

$$\varphi \equiv -\frac{\hat{\phi}_2(x', 0)}{\epsilon U_n L' \delta\lambda} = \mathrm{i}\frac{2k_1'}{B_n}\,\mathrm{e}^{\mathrm{i}k_1' x'}\int_0^{x'}(2x_1' - 1)G(x' - x_1')\,\mathrm{d}x_1' - 4B_n\,\mathrm{e}^{\mathrm{i}k_1' x'}\int_0^{x} G(x' - x_1')\,\mathrm{d}x_1' + 2B_n\,\mathrm{e}^{\mathrm{i}\mu\alpha x'} J_\circ(\alpha x'), \tag{5.10a}$$

and for $1 < x' < \infty$, as

$$\varphi(x, 0) = \mathrm{i}\frac{2k_1'}{B_n}\,\mathrm{e}^{\mathrm{i}k_1' x'}\int_0^1 (2x_1' - 1)G(x' - x_1')\,\mathrm{d}x_1' - 4B_n\,\mathrm{e}^{\mathrm{i}k_1' x'}\int_0^1 G(x' - x_1')\,\mathrm{d}x_1' + 2B_n\,\mathrm{e}^{\mathrm{i}\mu\alpha x'} J_\circ(\alpha|x'|) + 2B_n\,\mathrm{e}^{\mathrm{i}k_1'}\,\mathrm{e}^{\mathrm{i}\mu\alpha(x' - 1)} J_\circ(\alpha|x' - 1|), \tag{5.10b}$$

where

$$G(\xi) \equiv \mathrm{e}^{-\mathrm{i}(k_1' - \mu\alpha)\xi} J_\circ(\alpha\xi), \qquad \mu \equiv \frac{P}{2B_n^2\alpha}. \tag{5.10c, d}$$

There are two discontinuities in the surface velocity potential, at $x' = 0$ and $x' = 1$, which result from the transfer of the boundary condition for the N-wave.

Omitting the contribution of c/U in Ω, the parameter μ can be explicitly evaluated as

$$\mu = M_n \cos(\Lambda + \psi)/[1 - M_n^{-2}\sin^2(\Lambda + \psi)]^{1/2} \tag{5.10e}$$

which approaches M_n as $-\Lambda$ tends to ψ. Examination of (5.10*b*) reveals that $|\varphi(x, 0)|$ vanishes far downwind as $1/\sqrt{x'}$, in common with the Bessel function $J_0(\alpha\xi)$. The persistent, oscillatory wave pattern downwind ($x > 1$) can be found unambiguous by numerical evaluation, studied in Cheng *et al.* (2001). For a more general waveform, the f' assumed in (5.9) for the incident N-wave may be replaced by an arbitrary function regular in x' in [0, 1]. The simplicity of the N-wave example will allow an analytic delineation of the wave-field structure and its singularities, to be made in § 6.†

5.3. *Subsonic wave field underwater*

Elliptic PDE; synchronous solution

We seek a solution to the inverse underwater problem that can match the surface overpressure prescribed by the aerial wave field. For convenience, we again omit the prime and subscript n. After normalizing the overpressure by $\epsilon\rho_A U^2$, and anticipating a synchronous-type solution for the time-dependent part of the solution we obtain

$$p' = p_1' + \delta\,\hat{p}_2\,\mathrm{e}^{\mathrm{i}k_2' y'}\,\mathrm{e}^{-\mathrm{i}\Omega t} \tag{5.11}$$

where p_1' is the Sawyers solution in § 3. The PDE and its parameters governing $\hat{p}_2$ are the same as (5.7*a*, *b*, *c*), including the definitions of P and Q, except that the sound speed a is a_W pertaining to the water, and that $M_n < 1$; thus, the PDE is now elliptic.

Solution by Fourier transform

Allowing for the upwind influence, we solve the underwater problem for $\hat{p}_2$ via the Fourier transform in x':

$$\mathrm{FT}\,\hat{p}_2(x', z) = \frac{1}{\sqrt{2\pi}} \int_{-\infty}^{\infty} \mathrm{e}^{\mathrm{i}\xi x'}\,\hat{p}_2(x', z)\,\mathrm{d}x' \tag{5.12}$$

where FT signifies the Fourier transform operator. The existence of the Fourier transform of $\hat{p}_2$ and its inverse, as well as the applicability of the stationary-phase method for evaluating the large-z behaviour, will be more critically examined for the case of an incident N-wave in § 6. The Fourier transform of PDE (5.7*a*), with

$$\beta_n = \sqrt{1 - M_n^2} > 0,$$

and the assumption of $\hat{p}_2$ vanishing at large $|x'|$, yield an ordinary differential equation (ODE) for FT $\hat{p}_2$ in z:

$$\left(\frac{\partial^2}{\partial z^2} - K\right) \mathrm{FT}\,\hat{p}_2 = 0, \tag{5.13a}$$

$$K \equiv \beta_n^2 \xi^2 - P\xi - Q, \tag{5.13b}$$

where K depends on the Fourier variable ξ as well as on M_n, k_2' and k_1' or Ω through P and Q. The solution to this problem that can fulfil the attenuation requirement with respect to z, is

$$\mathrm{FT}\,\hat{p}_2 = \hat{A}(\xi)\sigma(\xi, z) \tag{5.14}$$

where $\hat{A}(\xi)$ is FT $\hat{p}_2$ at the reference interface $z = 0$:

$$\hat{A}(\xi) = \frac{1}{\sqrt{2\pi}} \int_{-\infty}^{\infty} \mathrm{e}^{\mathrm{i}\xi x'}\,\hat{p}_2(x', 0)\,\mathrm{d}x', \tag{5.15a}$$

† The results for an incident N-wave can be extended to an unbalanced N-wave by replacing $(2\xi - 1)$ in (5.9) by $[(a + 1)\xi - 1]$, $(2x_1' - 1)$ in (5.10*a*, *b*) by $[(a + 1)x_1' - 1]$, and the factor 2 of the last term of (5.10*b*) by $2a$.

and

$$\sigma(\xi, z) = \begin{cases} \exp(-\sqrt{|K|}z), & K \geqslant 0 \quad (5.15b) \\ \exp(\mathrm{i}\sqrt{|K|}z), & K \leqslant 0. \quad (5.15c) \end{cases}$$

The nonlinear relation among K^2, the frequency Ω (through P and Q) in (5.13b), and the Fourier variable ξ corresponds to the dispersion relation intrinsic to PDE (3.8a) that connects the wavenumber ξ to the frequency Ω. Equation (5.15b) for positive K shows an exponentially attenuating behaviour at large z, signifying therefore a horizontal propagation direction. The associated wave will be referred to as *horizontally propagating* wave component for this reason, although results with similar behaviours have been called 'evanescent waves' in optics and other fields. Equation (5.15c) for negative K indicates an unattenuated sinusoidal behaviour in z; the associated wave may therefore be called the *downward-propagating* wave component.

Whereas FT $\hat{p}_2$ at each ξ does not vanish individually at infinitely large z for the negative K, thanks to the mutual-cancellation (destructive influence) effect of the neighbouring sinusoidal components, their combined effect on $\hat{p}_2$, represented by the inverse transform, does attenuate with increasing z, as the analysis will confirm. In (5.15c), a specific choice has been made to ensure that the Fourier transform of the time-dependent part of p' (cf. (5.11), (5.14)) admits only downward-propagating waves away from the interface, giving

$$\mathrm{FT}\,\hat{p}_2\,\mathrm{e}^{-\mathrm{i}\Omega t} = \hat{A}(\xi)\exp\big[\mathrm{i}\big(|K|^{1/2}z - \Omega t\big)\big], \quad (5.16)$$

where Ω is positive, as noted earlier. It differs from the corresponding result in our earlier version (Cheng & Lee 1997, 1998) based on

$$\sigma = \cos\big(|K|^{1/2}z\big), \quad K \leqslant 0.$$

The solution for $\hat{p}_2$ is obtained by the inverse transform

$$\hat{p}_2 = \frac{1}{\sqrt{2\pi}}\int_{-\infty}^{\infty} \mathrm{e}^{-\mathrm{i}\xi x}\,\hat{A}(\xi)\sigma(\xi, z)\,\mathrm{d}\xi \quad (5.17)$$

which is a functional of FT $\hat{p}_2$ at $z = 0$; $\hat{A}(\xi)$, derivable from FT $\varphi(x, 0)$ via (5.8e):

$$\hat{A}(\xi) = \mathrm{i}\lambda[\xi + k_1']\,\mathrm{FT}\,\varphi(x, 0) + \mathrm{FT}\,(\Delta\hat{p}_{BT}), \quad (5.18)$$

where the subscript BT refers to the quantity resulting from transfer of the interface boundary condition (to the reference plane $z = 0$). In the form of (5.17) for $\hat{p}_2$, $\hat{A}(\xi)$ is seen as a surface source function resulting from the wavy-surface interaction. The last term in (5.18) represents the contribution resulting from the transfer of p_1 on the interface $z' = Z_W(x', t)$ to the reference plane $z = 0$ underwater (cf. (3.9b)), where $\partial p_1'/\partial z$ at $z = 0$ does not vanish, unlike that above water.

For an incident N-wave, we obtain†

$$\Delta\hat{p}_{BT} = -2\lambda\frac{\beta_n}{\pi}\,\mathrm{e}^{\mathrm{i}k_1'x'}\left[-2\ln\left|\frac{1-x'}{x'}\right| + (1-2x')\left(\frac{1}{x'-1} - \frac{1}{x'}\right)\right]. \quad (5.19a)$$

Employing an extended version of the Fourier integral theorem with suitable integration paths (e.g. Carrier, Krook & Pearson 1966, pp. 306–328) we arrive for the N-wave

† The second product term within the square bracket in (5.19a) can be written as $-(x')^{-1} - (x'-1)^{-1}$; a modification of (5.19a, b) for an unbalanced N-wave is included in Cheng & Lee (2000) Appendix IV.

at†

$$\mathrm{FT}\,\Delta\hat{p}_{BT} = \mathrm{i}\beta_n\lambda\sqrt{\frac{2}{\pi}}\,\mathrm{sgn}\,(\xi + k_1{}')\left[\mathrm{e}^{\mathrm{i}(\xi+k_1{}')}\left(\frac{2\mathrm{i}}{\xi + k_1{}'} + 1\right) - \frac{2\mathrm{i}}{\xi + k_1{}'} + 1\right]. \quad (5.19b)$$

The two pole singularities in (5.19*a*) at $x = 0, 1$ have resulted from the boundary-value transfer involving (shock) discontinuities. Their unbound values represent a local breakdown of the perturbation theory, but do not affect the uniform validity of the Fourier integral $\hat{A}(\xi)$ to the same order of Z_W or $\lambda\delta$ considered, and therefore do not affect the deep-water analysis which will depend explicitly on $\hat{A}(\xi)$. The suspected discrepancy caused by the non-uniformity in (5.19*a*) in the Fourier transform of (5.19*b*) come from transferring the boundary condition on the surface $z = Z_w(x', y', t)$ to the reference surface $z = 0$ by analytic continuation (cf. (3.9*b*)). The validity of (5.19*b*) has been established in Appendix IV of Cheng & Lee (2000) by an asymptotic matching analysis based on the complete form of (4.1*a*) for p. The resulting errors are shown to be much smaller than $(Z_W)^2$ or $(\lambda\delta)^2$.

5.4. *Far-field analysis: signals in deep water*

In the following, the deep-water field will be studied by analysing $\hat{p}_2(x', z)$ for a large z with the stationary-phase method. While several salient features could be inferred from some general knowledge of dispersive waves (Whitham 1974; Lighthill 1978), it is not obvious, however, if such knowledge will yield results applicable directly to the synchronous solution at hand, $\hat{p}_2\exp(-\mathrm{i}\Omega t)$, in which the frequency Ω is, in effect, fixed by U, k, and ψ. The issue of the consistency of the present results with known dispersive wave properties will be answered subsequently. Prior to a more thorough study, the parametric and spatial domains where the significant effect of interest can occur will first be identified.

Two distinct (Λ, ψ) domains

Owing to the distinctly different behaviour of the kernal function $\sigma(\xi, z)$ of (5.15*b*), depending on the sign of K, the contributions from the integrand to the solution integral of (5.17) differ widely for $K > 0$ and for $K < 0$. The two real roots of $K(\xi) = 0$ marking the transitions from the positive and negative K are (cf. figure 3*a*)

$$\xi_{1,2} = \frac{P}{2\beta_n^2} \mp \frac{1}{2\beta_n^2}\sqrt{P^2 + 4\beta_n^2 Q}, \quad (5.20a)$$

where the negative sign of $(\mp)$ will be identified with ξ_1, so that $\xi_1 < \xi_2$. For negligibly small c/u, the more explicit form of P and Q, (5.7*e*, *f*), can be used and the square root in (5.20*a*) becomes

$$S \equiv \sqrt{P^2 + 4\beta_n^2 Q} = 2k\sqrt{M_n^2 - \sin^2(\Lambda + \psi)}. \quad (5.20b)$$

This shows that those (unattenuated) sinusoidal components pertaining to $\xi_1 < \xi < \xi_2$ can occur only if

$$M_n^2 - \sin^2(\Lambda + \psi) > 0;$$

otherwise, the interval $[\xi_1, \xi_2]$ on the real ξ-axis cannot exist. (Note: $M_n < 1$ underwater.) Two parametric domains in (Λ, ψ) must therefore be distinguished for

† Professor S. N. Brown has indicated three alternative ways to arrive at the transformed result $\mathrm{i}\sqrt{\pi/2}\,\mathrm{sgn}\xi$ used here. Note, the principal value of the Fourier integral for $1/x'$ is taken (Titchmarch 1948).

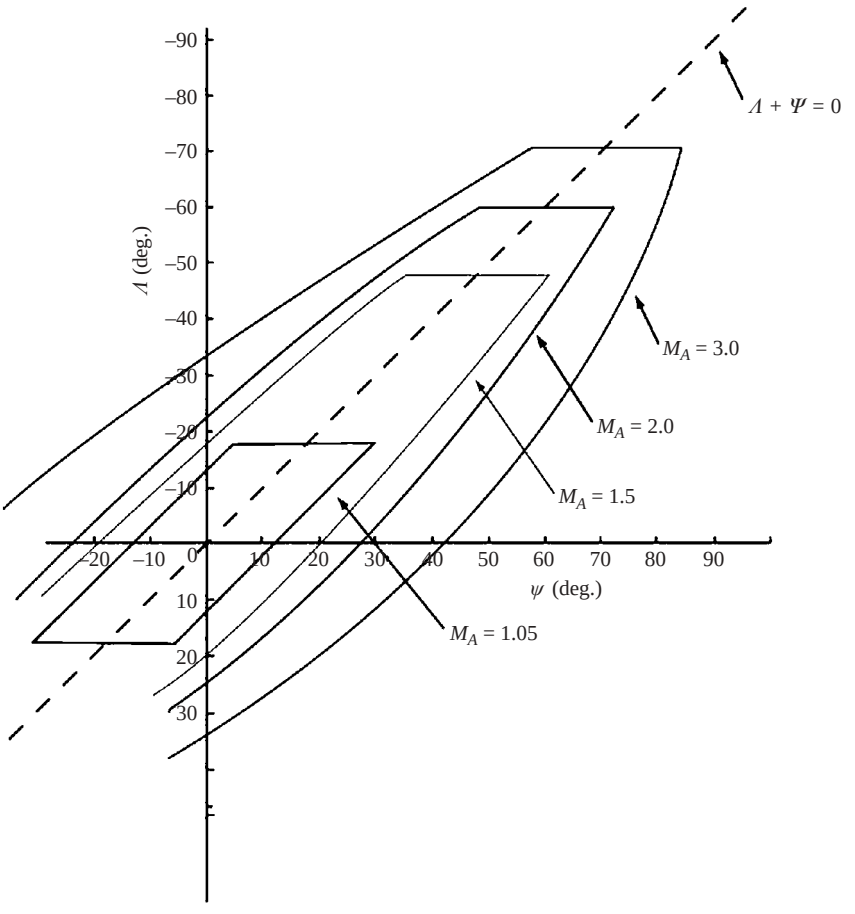

FIGURE 3. Boundaries in the (Λ, ψ) domain for different Mach numbers M_A, distinguishing the non-evanescent and evanescent acoustic fields, computed for $M_A \equiv U/a_A = 1.05, 1.5, 2.0$ and 3.0.

each M_n:

$$\left.\begin{array}{ll} \text{I.} & M_n^2 - \sin^2(\Lambda + \psi) < 0 \qquad \text{(Horizontally propagating),} \\ \text{II.} & M_n^2 - \sin^2(\Lambda + \psi) > 0 \qquad \text{(Downward propagating).} \end{array}\right\} \tag{5.21}$$

In Domain I, where the interval $[\xi_1, \xi_2]$ cannot exist on the real ξ-axis, $K > 0$ for all ξ components; it may be called the *horizontally propagating* domain in that the exponentially attenuating behaviour of (5.15*b*) with respect to z applies to all ξ-components. In this domain $|\hat{p}_2|$ from the inversion (5.17) attenuates with increasing z at an extremely high rate. Namely,

$$|\hat{p}_2| < \frac{|C|}{\sqrt{z}} \exp\left(-|K|_m^{1/2} z\right)$$

for an integrable $\hat{A}(\xi)$, where C is a constant and the subscript m refers to the minimum; therefore the resulting disturbances propagate mainly in the horizontal direction next to the surface. This behaviour may be inferred with help of the Laplace method or by the saddle-point method. More significant effects on $\hat{p}_2$ will therefore be found

in Domain II, in which an interval of real ξ can exist, and the sinusoidal (plane) waves components corresponding to (5.15*c*) are the principle contributors to the synchronous wave field at large z. This second domain will be called *downward-propagating* domain, even though there are wave components at $\xi < \xi_1$ and $\xi > \xi_2$ which attenuate exponentially with z.† Figure 3 gives boundaries delimiting the two district domains in (Λ, ψ) computed for four Mach numbers $M_A \equiv U/a_A = 1.05, 1.5, 2.0,$ and 3.0 based on the condition

$$M_n^2 - \sin^2(\Lambda + \psi) = 0 \tag{5.22a}$$

together with

$$\Lambda = \cos^{-1}(a_A/U). \tag{5.22b}$$

The latter condition is set by the limit of the Mach cone angle. The Domain II of interest lies in the area for each M_A enclosed by the boundary formed by the two curves from (5.22*a*) and by the line from (5.22*b*).

The downward-propagating domain: stationary phase

In Domain II, the inversion of the integral in (5.17) encompasses ranges over both the downward-propagating ($\xi_1 < \xi < \xi_2$) and the horizontally propagating ($\xi < \xi_1$, $\xi_2 < \xi$) components. While the contributions at large z from the evanescent segments exterior to $[\xi_1, \xi_2]$ is obviously small and secondary compared to that from the interior of $[\xi_1, \xi_2]$, their contribution at large z, though negligible, is by no means exponentially small like that from an individual evanescent component. This is because in approaching the end points of $\xi = \xi_1$ and $\xi_2 = \xi$, the function σ in (5.15*b*) can no longer vanish with increasing z, since

$$|K|^{1/2} \sim \text{const}|\xi - \xi_{1,2}|^{1/2}.$$

This leads, under the assumptions of an integrable $\hat{A}(\xi)$ and a finite x'/z, to a behaviour at large z comparable to the inverse square of the distance:

$$|\hat{p}_2| \sim |\text{const}|z^{-2}.$$

Integrable singularities of $\hat{A}(\xi)$ in the form of an inverse square root are anticipated from the asymptotic behaviour of the $J_0(\alpha\xi)$ of (5.10), for which the above estimate remains applicable except when one of these singularities coincides with the limit $\xi = \xi_1$ (see § 6.2 below). In this exceptional circumstance, the estimate becomes

$$|\hat{p}_2| \sim |\text{const}|z^{-1},$$

where we have made use of $\int_{-\infty}^{\xi_1} \mathrm{e}^{-\mathrm{i}\xi x}\, \mathrm{e}^{-|K|^{1/2}z} A(\xi)\, \mathrm{d}\xi \leqslant \int_{-\infty}^{\xi_1} \mathrm{e}^{-|K|^{1/2}z} |A(\xi)|\, \mathrm{d}\xi$, with similar consideration for the integral over ξ_2 and ∞. This is still small in magnitude compared to the contribution from $[\xi_1, \xi_2]$, to be shown below.

The integral of (5.17) over the remaining integration range corresponding to $K < 0$ may then be written for large z, subject generally to errors of the order z^{-2}, as

$$\hat{p}_2(x', z) \sim \frac{1}{\sqrt{2\pi}} \int_{\xi_1}^{\xi_2} \hat{A}(\xi)\, \mathrm{e}^{\mathrm{i}g(\xi)z}\, \mathrm{d}\xi \tag{5.23a}$$

† Wave components belonging to Domains I and II have been referred to as *evanescent* and *effervescent* waves, respectively, in Cheng & Lee (2000). The downward-propagating domain has also been called the *cylindrical-spreading* domain by Cheng, Lee and Edwards (2001).

where the function g is

$$g = |K|^{1/2} - \beta_n \eta \xi \tag{5.23b}$$

with

$$\eta \equiv x'/\beta_n z. \tag{5.23c}$$

The downward-propagating components corresponding to $\exp[\mathrm{i}g(\xi)z]\,\mathrm{d}\xi$ would have contributed to a non-vanishing $\hat{p}_2$ at large z, had there not been the mutual-cancellation (self-averaging) effect of the neighbouring components in the oscillatory phase $g(\xi)z$; the latter is made rapid by the large z. This mutual-cancellation effect results in a magnitude generally of order $\hat{A}/g'(\xi)z$. The exception is the contribution from the neighbourhood of ξ_* where the phase $g(\xi)$ is stationary, i.e. $g'(\xi_*) = 0$, and the destructive interference of the neighbouring wavenumber components is the least, thereby rendering a much reduced, slower attenuation rate with z. Lighthill (1978) called this a *re-enforcing mechanism* in selecting the least self-destructive wave mode. The root of $g'(\xi) = 0$ pertaining to the stationary phase is

$$\xi_* = \frac{P}{2\beta_n^2} - \frac{\sqrt{P^2 + 4\beta_n^2 Q}}{2\beta_n^2} \frac{\eta}{\sqrt{1+\eta^2}}. \tag{5.24}$$

The standard stationary-phase method under the assumption of a regular $\hat{A}(\xi)$ then gives along an arbitrary ray of fixed η

$$\hat{p}_2(x', z) \sim \hat{A}_* |g_*'' z|^{-1/2} \exp \mathrm{i} \left[g_* z + \mathrm{sgn}(g_*'') \frac{\pi}{4} \right] \tag{5.25}$$

where the double prime refers to the second ξ-derivative, and the subscript asterisk signifies values at the stationary phase $\xi = \xi_*$. Coefficients g_* and g_*'' are determined from P, Q and η, and (5.25) can be more explicitly expressed in $\bar{z} = \beta_n z$ and $\eta = x'/\beta_n z$ as

$$\hat{p}_2(x, z) \sim \frac{S^{1/2} \hat{A}(\xi_*)}{\sqrt{2}\beta(1+\eta^2)^{3/4}\sqrt{\bar{z}}} \exp \mathrm{i} \left[\frac{S}{2\beta_n^2} \left(\sqrt{1+\eta^2} - \frac{P}{S}\eta \right) \bar{z} - \frac{\pi}{4} \right] \tag{5.26}$$

where the parameters P and S can be evaluated from (5.7e) and (5.20b), respectively. In the above, the sum under the square root defining S is the same as $(P^2 - 4B_n^2 Q)$ in the definition of α in (5.8b), except that P and Q are evaluated here for $M_n < 1$ underwater. Accordingly, the overpressure due to the interaction attenuates with increasing depth as $1/\sqrt{\bar{z}}$, which corresponds to the cylindrical-spreading rule and is central to the present theory. Since ξ_* is bound by $\xi_{1,2}$ of (5.20), sonic disturbances reaching the deep water as predicted by (5.26) are limited mainly to the wavenumber range $[\xi_1, \xi_2]$ where $K < 0$, as in a bandfilter.

While inverse square-root singularities in $\hat{A}(\xi)$ are anticipated, they are not expected to occur within the interval $[\xi_1, \xi_2]$ and affect the uniform validity of (5.26). This will be ascertained by examining the analytical solution of $\hat{A}(\xi)$ for the incident N-wave case later in § 6.2.

In passing, we point out that the same result (5.26) can be obtained alternatively by the saddle-point method which calls for the construction of an analytic function for $\sigma(\xi, z)$ in the complex ξ-plane. This latter is accomplished with a suitable choice of branch cuts for $\sqrt{\xi - \xi_1}\sqrt{\xi_2 - \xi_*}$.

Wave packet, similitude, and group velocity

With the rapid oscillation for large z, the deep-water result exhibits traits familiar for dispersive wave in that the signals arrange themselves into a packet of quasi-sinusoidal

wavelets in a manner determined by the wavenumber ξ_* which, in this case, is the ξ value at the stationary phase along the ray $\eta = x/\bar{z}$, according to (5.26). The invariance of the wavenumber along the ray shown above may now provide a more satisfactory explanation of the $\hat{p}_2$ attenuation rate based on the cylindrical-spreading rule of the monochromatic waves. The result also implies a similitude in the spatial structure of the deep-water wave fields and their acoustic spectra, of which $\eta = x/\bar{z}$ is a similarity variable. Of theoretical interest is whether (the peak or valley of) the wavelet propagates at a speed and direction in agreement with the group velocity of the less restrictive wave system of PDE (3.8*a*). This will be delineated below.

It suffices for the present purpose to examine the case of $\Lambda = \psi = 0$, corresponding to the two-dimensional case, for which the dispersion relation relating the wavenumbers k, m and the frequency Ω of a progressive plane wave governed by PDE (3.8) $\exp[\mathrm{i}(kx + mz - \Omega t)]$ is

$$\Omega = Uk + a\sqrt{k^2 + m^2} \tag{5.27}$$

where the k is not to be confused with that used for the surface wavenumber of (5.1) and (5.2). The two group-velocity components are then given by the partial derivatives of Ω with respect to k and m as

$$\frac{x}{t} = U + \frac{k}{M(\Omega/a - Mk)}, \qquad \frac{z}{t} = U\frac{\sqrt{(\Omega/a - Mk)^2 - k^2}}{M(\Omega/a - Mk)} \tag{5.28a, b}$$

where $M = U/a$. The group-velocity propagation path is therefore

$$\frac{x}{z} = \frac{M[\Omega/a - Mk] + k}{\sqrt{(\Omega/a - Mk)^2 - k^2}}. \tag{5.29}$$

On the other hand, the synchronous pressure wave is $\hat{p}_2 \exp(-\mathrm{i}\Omega t)$, with $\hat{p}_2$ furnished by (5.25) or (5.26) as the result of the stationary phase $g'(\xi_*) = 0$. The latter condition identifies the wavenumber value ξ_* with a specific ray of constant $\eta = x/\bar{z}$ in (5.24). The inverse relation from (5.24) gives η as a function of the stationary wavenumber ξ_*, yielding

$$\frac{x}{z} = \frac{M(\Omega/a + M\xi_*) - \xi_*}{\sqrt{(\Omega/a + M\xi_*)^2 - {\xi_*}^2}} \tag{5.30}$$

for the ray slope which is the same as the group velocity propagation path (5.29) above, after identifying $-k$ with the Fourier variable ξ_*.

It remains to see if the constant-phase surface of $\hat{p}_2 \exp(-\mathrm{i}\Omega t)$ identified with a ξ_* also propagates along the ray $\eta = x/\bar{z}$ with the group velocity (5.28*a*, *b*). With (5.25) or (5.26), the oscillatory phase along constant η in question can be written for $\Lambda = \psi = 0$ as

$$\Psi = g_* z - \Omega t = \frac{\Omega}{\beta^2 a}\left[-\left(M - \frac{\eta}{\sqrt{1+\eta^2}}\right)x + \frac{\beta z}{\sqrt{1+\eta^2}} - \beta^2 a t\right]. \tag{5.31}$$

Upon substituting $\eta = x/\bar{z}$ and absorbing Ψ into a time shift, the contour of constant Ψ can be brought into the universal form

$$(x - Ut)^2 + z^2 = at^2. \tag{5.32}$$

A point on this surface must then propagate along the ray in a manner determined by the intersection of the curve (5.32) and the line (5.30); the result yields x/t and z/t as

functions of ξ_*, recognized precisely as the two group-velocity components (5.28a, b) after identifying k with $-\xi_*$.

In passing, we note that, whereas the frequency Ω is a constant throughout the entire synchronous field, the invariance of the wavenumber ξ_* along the group-velocity path is valid only under the far-field approximation (resulting from $\partial\xi_*/\partial x$ and $\partial\xi_*/\partial\bar{z}$ being both small like $1/\bar{z}$).

Significance

Comparing the time-dependent interaction effect p_2' with the flat-surface solution p_1', we arrive at an estimate of their relative magnitude (for fixed k and M_n):

$$\left|\frac{p_2'}{p_1'}\right| = O\left(\delta z^{3/2}\right). \tag{5.33}$$

Accordingly, the surface-wave correction will be comparable to the flat-surface wave field at

$$z = O\left(\delta^{-2/3}\right), \tag{5.34}$$

and become an effect of first-order importance at depths beyond this level.

We point out that the breakdown or non-uniformity of the perturbation procedure does not occur at large z, since the validity of the equations governing p_2' (3.8a, b) is unaffected by the vanishing far-field value of p_1'.

For a high k, the result (5.26), after omitting most unit-order factors, indicates that

$$|p_2| \sim \frac{\sqrt{k}\,\hat{A}(\xi_*)}{\sqrt{\bar{z}}}. \tag{5.35}$$

For incident N-waves and other similar waves, including those with unequal fore and aft shock jumps, it can be shown that

$$\hat{A}(\xi_*) = O\left(\frac{1}{k}\right) \tag{5.36a}$$

for larger k as will be unambiguously established for the N-wave in § 6.

Therefore $|p_2|$ may be scaled like the inverse square root of $(k\bar{z})$ for $k \gg 1$:

$$|p_2| = O\left(\frac{1}{\sqrt{k\bar{z}}}\right) \tag{5.36b}$$

for incident N-waves and other similar waves. Since $k\bar{z} = 2\pi\bar{z}/\lambda$, the result (5.36$b$) for $k \gg 1$ suggests that, if $\lambda \ll L'$, the effect in question is rather localized, and that the foregoing deep-water analysis is applicable as long as the depth level can be considered much greater than the smaller of λ and L'. These properties are substantiated by the more thorough analysis of the function $\hat{A}(\xi)$ for the case of an incident N-wave in § 6, as well as numerical studies in Cheng *et al.* (2001).

We would like to point out that the analysis (5.14)–(5.26) may also be used with $\hat{A}(\xi)$ determined from a subsonic wave field above water. One may consider for example the limit $U \to 0$, corresponding to a vanishing M_n both over and under the water. The time-dependent underwater overpressure p_2' based on $\hat{p}_2$ of (5.26), with $c \neq 0$ in Q, can be reduced to the form

$$G(\eta) r^{-1/2} \exp[\mathrm{i}\,(kr - \omega t)], \tag{5.37}$$

which is recognized as the cylindrical spreading of (monochromatic) multipole radiation from a source line.

The deep-water result (5.26) may be shown to be applicable also to a large $\eta \equiv x'/\bar{z}$ until $\eta = O(\bar{z})^{1/2}$, i.e. until $x = O(\bar{z})^2$. The $\hat{p}_2$ behaviour at η or x beyond these ranges may also be determined after some lengthy analysis. (Cheng & Lee 2000, Appendix II)

6. An explicit, analytic solution of $\hat{A}$ and its singularities

Singularities in the function $\hat{A}(\xi)$, particularly those at ξ_1, ξ_2 and $-k$, can be seen from (5.17)–(5.19). Of special concern are the singularities in $\hat{A}(z)$ resulting from Fourier transforms of the Bessel functions $J_0(\alpha x)$, $J_0(\alpha|x-1|)$ and related functions which give unbounded $\hat{A}(\xi)$ values, and could affect the uniform validity of p_2'. The following will identify these singularities and other analytical properties of $\hat{A}(\xi)$ on the basis of the exact result for an incident N-wave.

6.1. *An explicit form of* $\hat{A}(\xi)$

While the overpressure correction for the boundary condition transfer, $\Delta\hat{p}_{BT}$, has pole and logarithmic singularities generated by the front and tail shocks (cf. (5.19*a*)), its contribution to FT $\hat{p}_2(x,0)$ or $\hat{A}(\xi)$ obtained in (5.19*b*) turns out to yield only rather weak singularities at $\xi = -k$ where FT Δp_{BT} vanishes with a sign change in its derivative with respect to ξ. More critical are the singularities in the main part of FT $\hat{p}_2(x,0)$ through $\varphi(x,0)$ (cf. (5.18*a*)); its Fourier transform may involve those inverse square-root singularities, compounded further with the presence of discontinuities in $f'(x)$. The task of identifying these singularities is made simple by examining the $\hat{A}(\xi)$ for the incident N-wave, a completely analytic solution of which can be obtained. This is accomplished by recasting the integrals of (5.10*a*, *b*) into ones with the infinite integration range $[-\infty, \infty]$, employing the step (Heaviside) function concept; the final results were obtained by applying the convolution relation to the Fourier the transforms of these integrals with the help of Cauchy's integral formula, detailed in Cheng & Lee (2000, Appendix III). The complete analytical expression of $\hat{A}(\xi)$ for the incident N-wave example (omitting c/U from (5.18) as in (5.19)) is

$$\hat{A}(\xi) = \mathrm{i}\lambda(\xi + k_1')\,\mathrm{FT}\varphi(x,0) + \mathrm{FT}(\Delta p_{BT}); \tag{6.1}$$

the last term has been given by (5.19*b*) and

$$\mathrm{FT}\varphi(x,0) = \frac{1}{\sqrt{2\pi}\sqrt{R_1}\sqrt{R_2}}\left\{\mathrm{i}\frac{4k_1'}{B_n}\left[\frac{\mathrm{e}^{\mathrm{i}(\xi+k_1')}}{\xi+k_1'} + \mathrm{i}\frac{\mathrm{e}^{\mathrm{i}(\xi+k_1')}-1}{(\xi+k_1')^2} - \frac{1}{2}\frac{\mathrm{e}^{\mathrm{i}(\xi+k_1')}-1}{\xi+k_1'}\right]\right.$$
$$\left. - 4B_n\frac{\mathrm{e}^{\mathrm{i}(\xi+k_1')}-1}{\xi+k_1'} + \mathrm{i}2B_n\left(\mathrm{e}^{\mathrm{i}(\xi+k_1')}+1\right)\right\} \tag{6.2a}$$

where

$$R_1 \equiv \xi + \alpha(\mu+1), \quad R_2 \equiv \xi + \alpha(\mu-1), \tag{6.2b}$$

with μ given in (5.10*d*).

The result reveals three singularities in $\hat{A}(\xi)$, namely $\xi_{A1} = -\alpha(\mu+1)$, $\xi_{A2} = -\alpha(\mu-1)$ and $-k_1'$; their origin may be traced back to the (secondary) wave reflection from the extensively long surface wave train, and could have been apparent from the $\varphi(x',0)$ given in (5.10).

Accurate computation of $\hat{A}(\xi)$ by direct numerical evaluation of the Fourier integral of $\hat{p}_2(x',0)$, (5.15*a*), implemented with asymptotic expressions of the Bessel function

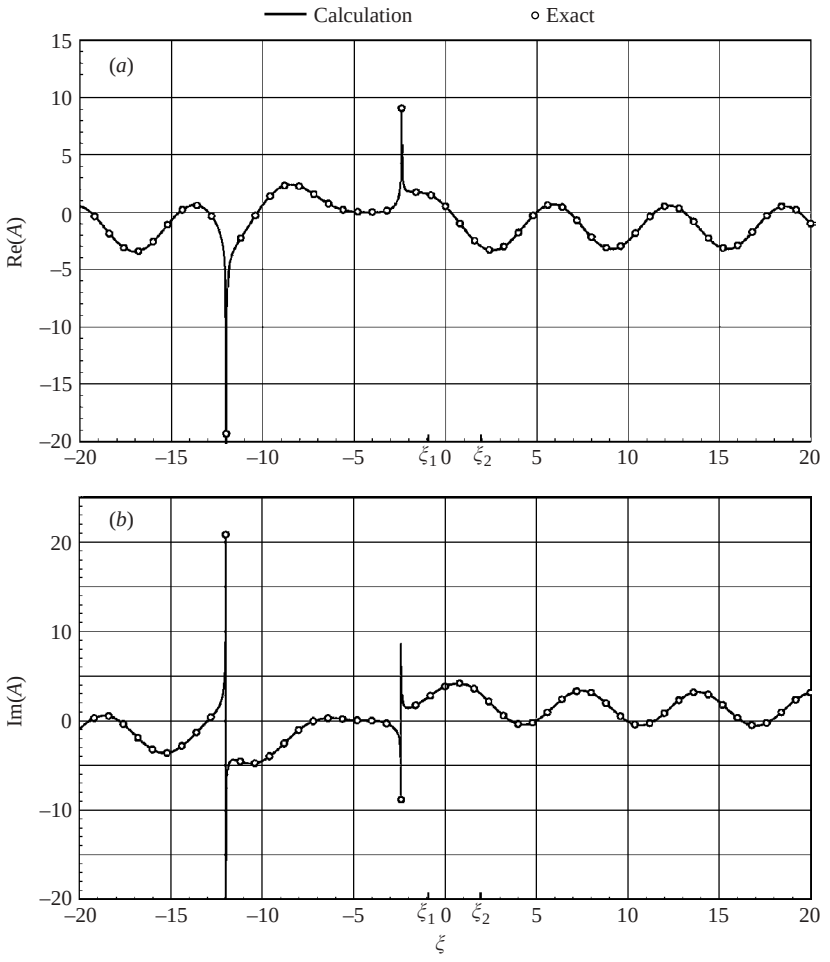

FIGURE 4. An example of $\hat{A}(\xi)$, the Fourier x'-transform of $\hat{p}_2(x', 0)$ for an incident N-wave, revealing its behaviour next to the two singularities at $\xi = \xi_{A1}, \xi_{A2}$. The result is for $k_1' = 4$, $M_{nA} = 1.5$ at $\Lambda + \psi = 0$, for which $\xi_{A1} = -12$ and $\xi_{A2} = -2.4$. The presence of the weaker singularity at $\xi = -k_1'$ is not apparent. (*a*) Real part, (*b*) imaginary part.

for large argument, agrees very well with the analytic expression (6.2). The distribution of $\hat{A}(\xi)$ exhibiting the behaviour near the two singularities $\xi_{A1}, \xi_{A2} = -\alpha(\mu \pm 1)$ is shown in figure 4(*a*, *b*) for a parameters set of μ, α, k_1', and B_n determined for the case of $M_n = 1.5, k_1' = 4$ and at $\Lambda = -\psi$ (where the surface wave train strikes the impact zone normally). The branch points ξ_{A1} and ξ_{A2} in this case are located at $\xi = -12$ and $\xi = -2.4$, respectively, confirming the behaviour seen in figure 4(*a*, *b*). The singularity at $\xi = -k_1'$ is too weak to be noticeable.

The nature of the three singularities of $\hat{A}(\xi)$ has now been ascertained. In spite of the prevalence of $(\xi + k_1')^{-1}$ and $(\xi + k_1')$ in (5.19*b*), (5.28*b*), the part $(\xi + k_1')\,\mathrm{FT}\,\varphi(x, 0)$ in $\hat{A}(\xi)$ of (5.28*a*) is regular at $\xi = -k_1'$, where $\hat{A}(\xi)$ is also to vanish but has a discontinuity in the second derivative contributed by FT Δp_{BT} of (5.19) from the boundary condition transfer, as noted.

We observe in passing that these singularities do not invalidate the inversion of $\hat{A}(\xi)\sigma(\xi, z)$ for $\hat{p}_2(x, z)$ via a path along the real ξ-axis according to (5.12), since $\hat{A}(\xi)$

is Riemann integrable. Along the real ξ-axis the product $R_1^{-1/2}R_2^{-1/2}$ is positive to the left of $\xi=\xi_{A,1}$, negative to the right of $\xi=\xi_{A,2}$, negatively imaginary above, and positively imaginary below the barrier/segment connecting $\xi_{A,1}$ and $\xi_{A,2}$.

The behaviour of $\hat{A}_*$ at large k may now be more explicitly shown with (6.1), (6.2*a*, *b*) for the incident N-wave as

$$\hat{A}(\xi;k)=\hat{A}(\bar{\xi}_*;k)=D_\infty(\bar{\xi}_*)\frac{1+\mathrm{e}^{\mathrm{i}k(1+\bar{\xi}_*)}}{k}, \tag{6.4a}$$

$$D_\infty(\bar{\xi}_*)=2\sqrt{2\pi}\left[\frac{1+B_n^2(1+\bar{\xi}_*)}{B_n\sqrt{\bar{R}_1^*}\sqrt{\bar{R}_2^*}}+\mathrm{i}B_n\,\mathrm{sgn}\,(1+\bar{\xi}_*)\right], \tag{6.4b}$$

where $\bar{\xi}_*\equiv\xi_*/k$, $\bar{R}_1^*\equiv R_1^*/k$ and $\bar{R}_2^*\equiv R_2^*/k$ are rescaled values of ξ, R_1 and R_2 at $\xi=\xi_*$, and become independent of k. The underwater properties of $|p_2'|$ at large k anticipated earlier in § 5 are thereby established for the case of an N-wave.

For a very low k corresponding to the limit $k\to 0$, or $\lambda\to\infty$, the $\hat{A}(\xi)$ distribution from (6.1), (6.2*a*, *b*) reduces to one that is precisely the Fourier transform of the quasi-steady part of the aerial solution $\hat{p}_2=f_2(x+Bz)$ at $z=0$ determined by the boundary condition (3.8*b*) or (5.6).

6.2. *The singularities and zeros of* $\hat{A}$*: solution validity*

The question of whether the deep-water result, (5.24*a*), in which $A(\xi_*)$ explicitly appears, could be affected by the foregoing singularities must be examined. For, if these singularities were to occur within the range $\xi_1<\xi<\xi_2$ for deep water, additional stationary-phase treatments would be needed. There are also ξ-values at which $\hat{A}$ and the deep-water p_2 envelope vanish.

The function $\hat{A}(\xi)$ will remain regular within the interval $[\xi_1,\xi_2]$ if ξ_1 can be shown to be greater than ξ_{A1}, ξ_{A2} and $-k_1'$. Analytical and numerical studies confirm that, in the domain of Λ, ψ and M_{nA} where the foregoing underwater analysis is applicable, $-k_1'$ is bound by ξ_{A1} and ξ_{A2}. It remains to ascertain if

$$\xi_{A2}<\xi_1, \tag{6.5}$$

which will ensure that the three singularities of $\hat{A}(\xi)$ cannot affect and invalidate the deep-water result (5.24). For this purpose, we examine the value of a function of M_{nA} and $\vartheta\equiv\Lambda+\psi$, which is a normalized form of $(\xi_{A2}-\xi_1)$:

$$\begin{aligned}F(\vartheta;M_{nA})&\equiv(1-\sigma^2M_{nA})\big(M_{nA}^2-1\big)(\xi_{A2}-\xi_1)\\&\equiv -M_{nA}^2(1-\sigma^2)\cos\vartheta+\big(1-\sigma^2M_{nA}^2\big)\sqrt{M_{nA}^2-\sin^2(\vartheta)}\\&\quad+\big(M_{nA}^2-1\big)\sqrt{\sigma^2M_{nA}^2-\sin^2(\vartheta)}\end{aligned} \tag{6.6}$$

and ascertain if F remains negative in the domain of interest as required by (6.5).

In either the limit of vanishing ϑ or vanishing $(M_{nA}-1)$, F is readily seen to be less than zero. For each M_{nA}, the maximum of F occurs at $\vartheta=0$, i.e. $\partial F/\partial\vartheta=0$ and $\partial^2F/\partial\vartheta^2<0$; The location of the impact zone where ξ_{A2} gives the closest approach to ξ_1 is therefore at $\vartheta=0$, whereas the span stations with the largest negative F or $(\xi_{A2}-\xi_1)$ are found in the limit $\Lambda+\psi=\sin^{-1}(\sigma M_{nA})$ corresponding to the square-root singularity of $F(\vartheta, M_{nA})$ in (6.6). These properties substantiated by extensive computation of $F(\vartheta;M_{nA})$ for several Mach numbers confirm that the inequality $\xi_{A2}<\xi_1$

indeed holds. The conclusion from the foregoing discussion may therefore be summarized by the inequalties

$$\xi_{A1} < -k_1' < \xi_{A2} < \xi_1 < \xi_2 \tag{6.7}$$

Hence, these three singularities of $\hat{A}$ cannot invalidate the foregoing deep-water analysis, (5.20)–(5.26), in which the stationary phase occurs well inside $[\xi_1, \xi_2]$. Some influence of singularities in $\hat{A}(\xi)$ is expected in the wave field at a finite depth, nevertheless. Other $\hat{A}(\xi)$ behaviours for the N-wave may also be of interest. The third singularity, namely $\xi = -k_1' = -k\cos(\Lambda + \psi)$, is interesting in that the function $\hat{A}(\xi)$ actually vanishes at $\xi = -k_1'$ with a rather weak singularity. There are ξ-values, however, at which $-\mathrm{i}\lambda(\xi + k_1')\,\mathrm{FT}\,\varphi(x, 0)$ and $\mathrm{FT}\,\Delta\hat{p}_{BT}$ both vanish and so will $\hat{A}(\xi)$. Some of these zeros occur within $[\xi_1, \xi_2]$ and will therefore reveal their presence in the waveform envelope for deep water. The location of these zeros in the ξ-range, or in the η-range (via (5.24)), can be determined from the condition for the vanishing of $\mathrm{FT}\,\varphi(x, 0)$. Detailed examination shows that the set of zeros of $\hat{A}(\xi)$ is given by the origin of $\nu = \xi + k_1'$ (cf. (6.2*a*)) together with the intersection of $(\nu/2)$ and $\tan(\nu/2)$.

The vanishing of $|\hat{A}(\xi)|$ at the intersection of $\nu/2$ with $\tan(\nu/2)$ provides a concrete basis for explaining and predicting the zero-crossing points of $\hat{A}(\xi)$ in figure 4(*a*, *b*). In particular, the locations where $|\hat{A}(\xi)| = 0$ shown for the example $k = 4$, $M_{nA} = 1.5$ and $\Lambda + \psi = 0$ are found to be closely identified with $\xi = -7.20, -4, 5.42, 11.7$ and 18.0. Note that $\hat{A}(\xi) = 0$ requires the vanishing of both the real and imaginary parts of $\hat{A}$, therefore some of the zero-crossing points appearing in figures 4(*a*) and 4(*b*) are not the zero in question. One may also note that not the entire family of the zero-crossing ξ-values can be expected to effect wave-envelope quenching in deep water through the $\hat{A}(\xi_*)$ in (5.24), since the range of ξ_* is restricted by ξ_1 and ξ_2.

7. Acoustic pressure and energy spectra in the rest frame

The study in the last two sections delineates the waveform at large z in the moving frame. The corresponding waveform and frequency spectrum in the rest frame are nevertheless of practical interest; some of their properties will be examined below.

7.1. *Time-dependent description in a rest frame*

With the normalized time $\tilde{t} = Ut/L'$, and other dimensionless variables and parameters unchanged, the x'-coordinate in the moving frame is related to the $\underline{x}$-coordinate and time $\tilde{t}'(=\tilde{t})$ through

$$x = \underline{x} + \tilde{t}, \quad y = \underline{y}, \tag{7.1a}$$

and

$$x' = x\cos\Lambda - y\sin\Lambda, \quad y' = x\sin\Lambda + y\cos\Lambda, \tag{7.1b}$$

where x and y are taken as local Cartesians. It is convenient to locate the origin of the reference station in the rest frame at $\underline{x} = \underline{y} = 0$ and interpret η in the rest frame to be a *normalized time* at each depth level $\bar{z}$:

$$\eta \equiv \frac{x'}{\bar{z}} = \frac{\tilde{t}\cos\Lambda}{\bar{z}}. \tag{7.2a}$$

The synchronous-time factor in (5.2*a*), (5.11) may now be expressed as

$$\mathrm{e}^{-\mathrm{i}\Omega t} = \exp[-\mathrm{i}k(\cos\psi)\tilde{t}]. \tag{7.2b}$$

In terms of the normalized time η, the overpressure p_2 from the interaction, with $\hat{p}_2(x', z) = \hat{p}_2((\eta, \bar{z}))$, may be expressed as

$$p_2 = \hat{p}_2((\eta, \bar{z}))\mathrm{e}^{-\mathrm{i}\cos\psi\,\sec\Lambda k\eta\bar{z}} \tag{7.3}$$

where $\eta\bar{z}$ may be identified with $\tilde{t}\cos\Lambda$ or x'.

7.2. *Fourier transform of p_2 with respect to time: acoustic energy spectral density*

With p_2 given above, we shall examine its Fourier transform with respect to time

$$\mathscr{F}t(p_2) \equiv \frac{1}{\sqrt{2\pi}}\int_{-\infty}^{\infty} \mathrm{e}^{\mathrm{i}\bar{\omega}\tilde{t}}\, p_2\, \mathrm{d}\tilde{t} \tag{7.4}$$

where $\bar{\omega}$ is now a dimensionless Fourier t-transform parameter, recognizable as a radian frequency normalized by U/L' (as for Ω). This is recognizable also as the same as the Fourier x'-transform of $\hat{p}_2(x', \bar{z})$ with the Fourier variable ξ therein replaced by

$$\begin{aligned}\bar{\Omega} &\equiv (\bar{\omega} - \Omega)\sec\Lambda + k_2' \tan\Lambda \\ &= \bar{\omega}\sec\Lambda - k\cos(\Lambda + \psi).\end{aligned} \tag{7.5a}$$

Namely,

$$\begin{aligned}\mathscr{F}t(p_2) &= \frac{\sec\Lambda}{\sqrt{2\pi}}\int_{-\infty}^{\infty} \mathrm{e}^{\mathrm{i}\vartheta x'}\,\hat{p}_2(x', \bar{z})\,\mathrm{d}x' \\ &= \hat{A}(\bar{\Omega})\sigma(\bar{\Omega}, z)\sec\Lambda\end{aligned} \tag{7.5b}$$

where, according to (5.14) and (5.20), the function σ is $\exp(\mathrm{i}|K(\bar{\Omega})|^{1/2})$ for $\xi_1 < \bar{\Omega} < \xi_2$, and is $\exp(-|K|^{1/2}\bar{z})$ otherwise.

The absolute value of $\mathscr{F}t(p_2)$ expressed as a function of $\bar{\omega}$ may be referred to as the *acoustic-pressure spectrum* and is to be evaluated for the present problem as

$$|\mathscr{F}t(p_2)| = |\hat{A}(\bar{\Omega})||\sigma(\bar{\Omega}, z)|\sec\Lambda. \tag{7.6a}$$

Its square, $|\mathscr{F}t(p_2)|^2$, represents an acoustic energy flux as a function of $\bar{\omega}$ and may be called the *acoustic energy* (*exposure*) *spectral density*, following a convention in the acoustic literature. The rationale for this notion may be found in its formal relation with the total energy of an acoustic pulse via the convolution

$$\int_{-\infty}^{\infty} |p_2|^2\,\mathrm{d}t = \int_{-\infty}^{\infty} |\mathscr{F}tp_2|^2\,\mathrm{d}\bar{\omega}, \tag{7.7}$$

referred to as the (*total*) *acoustic* (*energy*) *exposure* (Pierce 1991; Tolstoy & Clay 1966, 1987; Medwin & Clay 1998). The convolution relations for p_2 in (7.7) and in (7.8) below are applicable also for the real part of p_2.

We noted from (6.2) that $\hat{A}(\xi)$ has inverse square-root singularities at $\xi = \xi_{A1}, \xi_{A2}$ and does not vanish as $\xi \to \infty$. Therefore $|\mathscr{F}t(p_2)|$ and $|\mathscr{F}t(p_2)|^2$ for $z = 0$ are unbounded at $\bar{\Omega} = \xi_{A1}, \xi_{A2}$ and non-integrable in the limits $|\omega| \to \infty$ (apart from being non-integrable at $\bar{\Omega} = \xi_{A1}, \xi_{A2}$ for $|\mathscr{F}t(p_2)|^2$). This suggests that an infinite amount of energy has been extracted from the incident sonic-boom wave by the infinite wave train of our model since the interaction has begun long ago at $t = -\infty$. The solution of p_2 as well as $|p_2|$ at $z \neq 0$ underwater is nevertheless finite and regular since $\hat{A}(\xi)$ under the inverse Fourier transform of (5.17) is integrable.

Owing to the non-integrability of $|p_2|^2$ and $|\mathscr{F}t(p_2)|^2$ noted above, the total exposure integral (7.7) is generally meaningless but is nevertheless meaningful in deep water,

for which the acoustic energy associated with the interval $[\xi_1, \xi_2]$ remains unfiltered, with interesting consequence.

7.3. *Deep-water signature in the rest frame*

For deep water, the overpressure p_2 of (7.3), with $\hat{p}_2(\eta, \bar{z})$ given by (5.26), yields a time-domain wave packet in the rest frame described by the slow time variable $\eta = t/\bar{z}\sec\Lambda$ and a fast time variable proportional to $\bar{z}$, which is the oscillatory phase itself. While the wave packet envelope is modulated through η, the modulation in the oscillatory phase is characterized by a frequency downshift, i.e. the oscillation frequency decreases with increasing time during the sound source passage, as anticipated from Doppler's principle. This is most readily seen in the case of $\Lambda = \psi = 0$, for which, with $\hat{A}(\xi_*) = \hat{A}((\xi, \bar{z}))$,

$$p_2 \sim \frac{\sqrt{kM_w}\hat{A}((\eta, k))}{\beta_w(1+\eta^2)^{3/4}(\bar{z})^{1/2}} \exp \mathrm{i}\left[\frac{k\bar{z}}{\beta_w{}^2}(M_w\sqrt{1+\eta^2} - \eta) - \pi/4\right]. \tag{7.8}$$

Recall that ξ_* is the stationary-phase value of ξ determined by η in (5.24). Therefore, $\mathscr{F}t(p_2)$ in (7.5) as a function of $\bar{\omega}$ through ϑ must also be taken as a function of the normalized time η through $\bar{\Omega} = \xi_*(\eta)$. This can be shown to be valid by evaluating $\mathscr{F}t(p_2)$ directly from the deep-water result of $\hat{p}_2$, (5.24). Therefore the spectrum in this case carries a time record for $\mathscr{F}t(p_2)$, revealing how the complex function $\mathscr{F}t(p_2)$ has evolved since time began at $t = -\infty$. The frequency $\bar{\omega}$ of the spectrum corresponding to $\bar{\Omega} = \xi_*(\eta)$ may hence be denoted by $\bar{\omega}_*(t)$ and possesses a genuine physical meaning as an instantaneous frequency which varies on a time scale comparable to the pulse duration. It can be readily shown to be the rate (of decrease) of the (rapidly) oscillating phase of $\hat{p}_2$ at t in deep water, with the help of (5.26) with (7.2*b*).

It follows from (5.26) with (5.24) that

$$\begin{aligned}\int_{-\infty}^{\infty} |p_2|^2 \,\mathrm{d}\tilde{t} &= \bar{z}\sec\Lambda \int_{-\infty}^{\infty} |p_2|^2 \,\mathrm{d}\eta \\ &= \sec\Lambda \frac{\mathscr{S}}{2\beta_n^2} \int_{\xi_1}^{\xi_2} \frac{|\hat{A}(\xi_*)|^2}{(1+\eta^2)^{3/2}} \left(\frac{\mathrm{d}\eta}{\mathrm{d}\xi_*}\right) \mathrm{d}\xi_* = \sec\Lambda \int_{\xi_1}^{\xi_2} |\hat{A}(\xi_*)|^2 \,\mathrm{d}\xi_*. \end{aligned} \tag{7.9a}$$

Hence, at large $\bar{z}$, and noticing that $|\mathscr{F}t(p_2)| = \sec\Lambda|\hat{A}(\vartheta)|$, we arrive at

$$\int_{-\infty}^{\infty} |p_2|^2 \,\mathrm{d}\tilde{t} = \int_{\bar{\omega}_1}^{\bar{\omega}_2} |\mathscr{F}t(p_2)|^2 \mathrm{d}\bar{\omega} \tag{7.9b}$$

where the two integration limits can be determined from (7.5*a*) with (5.7*e*) and (5.20*a*) as

$$\begin{aligned}\bar{\omega}_{1,2} &= \cos\Lambda\xi_{1,2} + k\cos(\Lambda+\psi)\cos\Lambda \\ &= \frac{k\cos\Lambda}{\beta_n^2}\left[\cos(\Lambda+\psi) \mp \sqrt{\cos^2(\Lambda+\psi) - \beta_n^2}\right] > 0. \end{aligned} \tag{7.9c}$$

Therefore, the magnitude squared of the Fourier x'-transform of $\hat{p}_2$ at the sea level ($z = 0$), with the argument ξ therein replaced by $\bar{\Omega}$, becomes the *acoustic exposure* spectral density in deep water. Comparing (7.9*b*) with the formal integral relation (7.7), not only are the $|\mathscr{F}t(p_2)|^2$ made more explicit, and the frequency range limited to only $[\bar{\omega}_1, \bar{\omega}_2]$, but, unlike (7.7), the total energy exposure reaching deep water is shown to be finite and depth independent (for a sufficiently large $\bar{z}$).

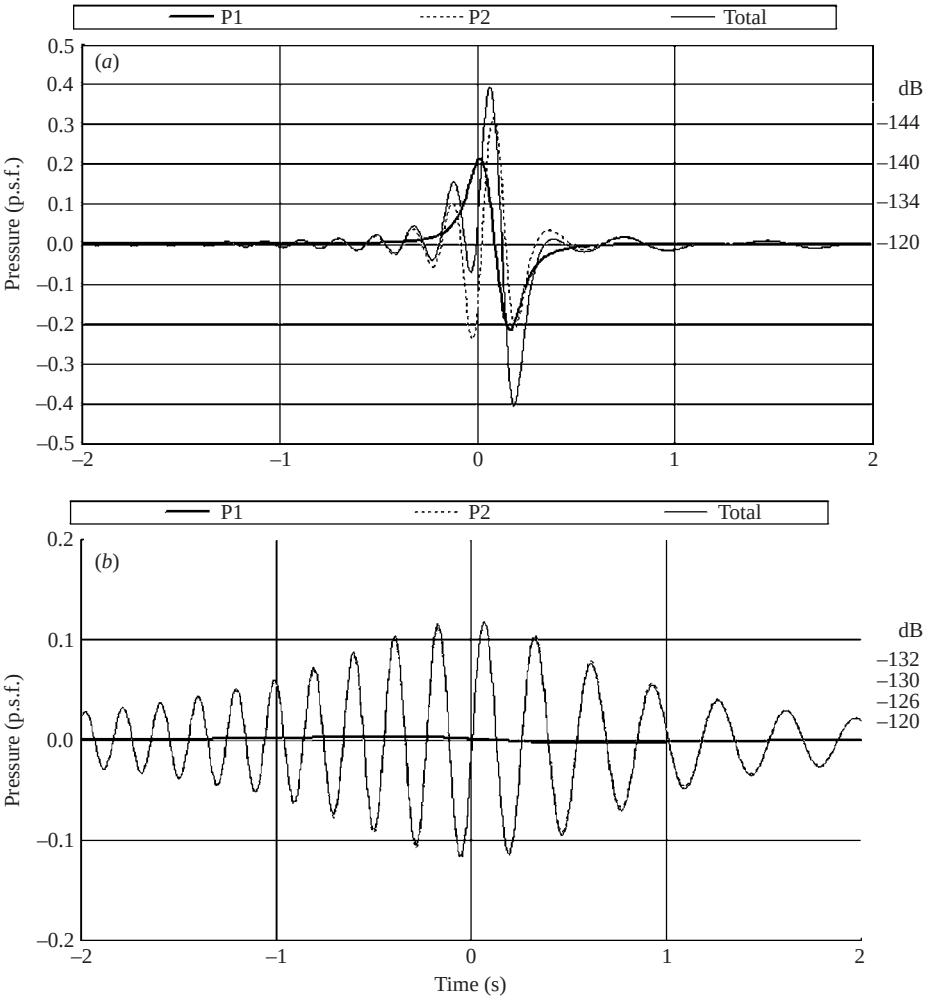

FIGURE 5. An example of the underwater overpressure waveform produced by an N-wave with $M_A = 1.5$, surface-wave wavenumber $k = 4$, maximum wave slope $\delta = 0.025$, sea-level signature length $L' = 300$ ft, and max. sea-level overpressure 2 p.s.f., at two depth levels: (*a*) $zL' = 150$ ft and (*b*) $zL' = 1500$ ft.

8. An example

Before closing, an example is shown to illustrate the surface-wave effect on sonic-boom penetration depth, and the perceivable sound level, frequency range and waveform characteristics. While more extensive application studies pertaining to much wider parameter domain are documented in Cheng *et al.* (2001), this example suffices for indicating the significant wavy-surface influence that will affect the noise audibility issue of interest. The results were obtained for an N-wave of surface Mach number $M_A = 1.5$ incident upon a sinusoidal surface-wave train with surface wavenumber $k = 4$ and a maximum wave slope $\delta = 0.025$. The study assumes a reference length $L' = 300$ ft (~ 90 m) not far from the signature length of a typical supersonic transport, and a maximum overpressure on the otherwise flat surface of 2 pounds per square feet (p.s.f). Overpressure waveforms shown in figures 5(a, b), were computed from the inverse Fourier transform of the product $\hat{A}\sigma$, using the $\hat{A}$ for $M_A = 1.5$ and $k = 4$ shown

earlier in figures 4(a, b) for two depth levels: 150 ft ($z = 0.5$) and 1500 ft ($z = 5$) directly under the flight track ($\Lambda = 0$). It is also assumed that the surface-wave propagation direction aligns closely with the flight track in this case ($\psi = 0$). The examination also affords an opportunity to compare with results from Sawyers' flat-surface model and from the far-field formula (7.8) applicable to deep water.

Whereas the wavy-surface interaction effect is expected to be small and secondary to Sawyers's prediction at depth levels comparable to the signature length ($z = O(1)$), the data from the time-dependent wavy-surface effect p_2' (dotted line) shown in figure 5(a) for $z = 0.5$ is far from being a secondary quantity even at a depth of half of the signature length. The resultant overpressure $p' = p_1' + p_2'$ (thin solid line) therein is seen to be more than double the flat-surface value p_1' (solid curve) at the peak, with noticeable undulations ahead of and behind the peak. At a depth level five times the signature length ($z = 5$), p_2' takes the dominating form of a wave packet, overwhelming the flat-surface waveform p_1', as predicted by the theory. Figure 5(b) compares the resultant overpressure p' with the Sawyers solution p_1 at $z = 5$; the p_2' at this depth is too close to be distinguishable from the p' at this depth and is not included. According to this calculation, the audible sound level from the incident N-wave at $z = 5$, by virtue of its interaction with the surface-wave train, is not low; the averaged peak level of the wavelets over the 4 s (pulse) duration shown is well above 0.02 p.s.f. ~ 120 dB (re 1 μPa) with the maximum peak level slightly above 0.10 p.s.f. ~ 134 dB (re 1 μPa).† The sound frequency from the nearly monochromatic, sinusoidal wavelets, as inferred from the time interval between peaks, is seen to fall in the near infrasound range, varying from an average of 5 Hz before the maximum peak to an average of 3 Hz after the maximum peak. The far-field formula (7.8) has been applied to determine the deep-water waveform at $z = 5$ in this case; the result is graphically indistinguishable from p_2' of figure 5(b) and is therefore not shown.

Since the p_2' magnitude at $z = 5$ is scaled by the surface-wave slope δ, the results in figures 5(b) for $\delta = 0.025$ can be used to indicate that a sound pressure levels above 120 dB (re 1 μPa) may still reach the same depth even for a surface-wave slope five-fold smaller, i.e. $\delta = 0.005$. Waveforms with similar frequency downshift characteristics are found consistently in examples for higher M_A and k, with expected increases in sound pressure and in dominant frequency (Cheng *et al.* 2001).

9. Summary and discussion

The foregoing analysis shows that interaction of a sonic boom with a wavy air–water interface produces time-dependent disturbances which can penetrate much more deeply underwater than with a (non-wavy) flat-ocean model. The problem is formulated for a high water-to-air density ratio, and a water-to-air sound speed ratio greater than unity; a surface-wave train with small slope is considered and the aspect ratio of the sea-level impact zone (in the sense of § 3.1 and figure 2) is assumed to be very high. While the overpressure ratio ϵ is assumed small, no restriction is required under the parametric requirement in § 3.1 on the relative magnitudes of ϵ and the surface slope $2\pi\delta$. The analysis is made in a coordinate system moving with the incident wave field and addresses the time-dependent interaction in which the primary underwater wave field is subsonic ($U \cos \Lambda / a_W < 1$).

† The dB unit for the sound pressure level is evaluated from dB (re 1 μPa) $= 20 \log_{10}(|p'|/\mu\text{Pa})$.

The study focuses on the problem of an N-wave incident upon a sinusoidal surface-wave train, for which wave-field features can be delineated analytically and the solution validity more firmly established. The interaction produces a time-dependent surface acoustic source corresponding to a surface overpressure with a continuous wavenumber spectrum. Far below the surface, waves of downward-propagating type (§ 3.4) dominate and disperse into a wavepacket form. The latter has a similarity structure with two distinct time scales: at a fixed depth, amplitude and frequency of the wavelet are seen to vary (among the wavelets) much more slowly than the wavelet oscillation frequency itself; along a ray of constant $\eta = t/z$ (in the rest frame) or x/z (in the moving frame), on the other hand, the amplitude and frequency are found to be invariant, after being rescaled with $1/\sqrt{z}$ and z, respectively.

Of significance is the $1/\sqrt{z}$ behaviour of the overpressure that attenuates far more slowly with depth than the corresponding $1/z^2$ behaviour in the flat-ocean (Sawyers) model. Thus the surface-wave influence, even though a small secondary effect near the surface, becomes an effect of first-order importance in deep water and eventually overwhelms the otherwise primary wave field. This was demonstrated by the example studied in § 8 and figures 5(a, b) and is substantiated by studies with many other examples in Cheng *et al.* (2001), and in laboratory experiment as well (Fincham & Maxworthy 2001).

Viewed in the moving frame, results from the foregoing analysis for deep water may be anticipated in part as dispersive-wave properties. For the wave group propagating far from the source, the individual wave component progresses in a direction and a velocity determined by the wavenumber ξ_* of the stationary phase, and the wave group as a whole disperses into the form of a packet of wavelets, each of which retains its monochromic characteristics pertaining to ξ_*. The two-dimensional divergent paths of the neighbouring wavelets must then cause the wavelet amplitude to reduce with increasing distance, in the same manner as the attenuation of cylindrical waves from a monochronmatic point source. Thus, the agreement of our results with general properties expected from dispersive waves, in regard to the wavenumber invariance (along propagating path) and the group velocity, should not be unexpected.

Since the frequency in the sound-pressure spectrum in deep water is a function of a slow time variable, the spectrum of the entire pulse is seen to build up in (slow) time successively from one (narrow) frequency band to the next during the entire pulse-passage period (which is many times longer than the sea-level sonic-boom pulse period). In view of the frequency downshift observed in § 8 and figures 5(a, b), the higher frequency end of the spectrum will be the first to appear. Thanks to the frequency/wavenumber cut-off on the non-evanescent waves, the deep ocean serves as a bandfilter and makes the total acoustic energy exposure (cf. (7.8b)) as well as the acoustic exposure spectral density, $|\mathscr{F}t(p_2)|^2$, finite and depth independent.

Among the parametric requirements expected to be important for field observations and laboratory simulations are the considerations that distinguish the (Λ, ψ) domain of interest from the one supporting strictly evanescent waves. The examinations in § 5.4 and figure 4 indicate that acoustic signals from wavy-surface interaction may not be detectable if the flight Mach number M_A is too close to unity, or the surface-wave propagation direction ψ too far from the flight direction. This, together with the unexpectedly high level of ambient noise, may explain the lack of detectable wavy-surface effect in Sohn *et al.*'s (1999) field measurement.

By virtue of the weak nonlinearity in the basic formulation, more general cases other than the incident N-wave and the sinusoidal surface-wave train can be analysed;

superpositions of wave trains of different surface wavelengths and horizontal propagation directions are expected to yield interference pattern, with interesting consequences.

The surface-wave wavelength λ and the reference sonic-boom signature length L' used in defining the surface-wave wavenumber $k = 2\pi L'/\lambda$ vary according to the sea states and the type of aircraft/space vehicles considered. Taking λ in the range of $20 \sim 100$ m, k for aircraft can be as low as unity and as high as 30, while for rocket space launch, k can be in the range of 20 to 80 or higher. Apart from k, the sound level is also controlled by the surface slope parameter δ and the surface Mach number M_A. Examples in wide ranges of k, δ, and M_A for incident N-waves and other sonic-boom waves were examined in Cheng *et al.* (2001).

This work has been motivated by the need to improve the models for the analysis of underwater sonic-boom noise which may potentially harass marine mammals. Noteworthy is perhaps the 10–50 Hz frequency range found in examples in deep water studied here and in Cheng *et al.* (2001). This infrasound range is believed to be the main channel of long-distance calls for Fin and Blue whales and other large undersea mammals (Richardson *et al.* 1995; Frankel & Clark 1997). The examples indicate that sound levels in the range of 100 to 130 dB (re 1 μPa) can be found at depth down to five signature lengths, which includes the 120 dB (re 1 μPa) that is an important reference level in marine mammal avoidance behaviour studies (NRC 1992; D'Spain *et al.* 1995). Of interest in this regard is the tonal-variation found with the frequency downshift and the long duration of the wave packet at large depth levels. Finally, it remains to be ascertained whether undersea ambient noise may significantly affect the signal audibility. The accepted, averaged, ambient-noise level in deep sea is seen to level off over the 10–50 Hz frequency range at the sound intensity level of 60–80 dB (re 1 Pa/$\sqrt{\text{Hz}}$), depending on ocean traffic and wind conditions (Wentz 1962; Urick 1983; NRDC 1999; also Munk *et al.* 1995).† Its effect on the predicted audible signals will also depend on the exposure time allowed by the hearing device/mechanism, and shall be investigated.

In closing, we point out that the influence of the sea floor, not treated in this part of the study, will be an important topic concerning the sonic-boom impact on shallow coastal water, where the interaction with seismic/elastic waves on the sea-bed sediment represents an outstanding issue, as suggested in the studies by Desharnais & Chapman (1998), and more recently, by Cheng, Kunc & Edwards (2004).

The authors would like to express their appreciation of the helpful discussions on several parts of this study with A. Bowles, S. Brown, G. Carrier, C. S. Clay, G. D'Spain, J. R. Edwards, A. Fincham, C. R. Greene, R. Kaplan, G. N. Malcolm, T. Maxworthy, H. Medwin, K. Plotkin, L. Redekopp, V. Sparrow, R. Sohn and B. Sturtevant. The study was supported in part by the Ocean Sonic Boom Program monitored by Los Angeles AF SMC Environment Management Div. at HKC Research through Parsons Engineering Sciences, Subcontract 73824903000-02. Earlier support by a DoD SBIR program through AF Armstrong Laboratories Noise Effect Branch is also acknowledged.

† The $60 \sim 80$ dB (re 1 μPa) in Wentz's and Urick's work was presented for data based on the frequency interval of one (1) Hz. For the signal received from a pulse-duration of 10 s, the effective ambient noise level must accordingly be raised to $70 \sim 90$ dB (re 1 μPa), which is still well below the $100 \sim 130$ dB (re 1 μPa) range found here.

REFERENCES

Ashley, H. & Landahl, M. 1968 *Aerodynamics of Wings and Bodies*. Addison-Wesley.

Au, W. W. L., Nachtigal, P. E. & Powloski, K. L. 1997 *J. Acoust. Soc. Am.* **101**, 2973–2977.

Bascom, W. 1964 *Waves and Beaches*, pp. 9–11, 42–59. Education Service, Inc.

Bowles, A. E. 1995 Effects of sonic booms on marine mammals:problem review and recommendation on research. *Proc. NASA Sonic Boom Workshop, NASA Conf. Pub.* 3335.

Bowles, A. E. & Stewart, B. 1980 Disturbances to pinnipeds and birds of San Miguel island, 1979–1980. *Tech. Rep.* 81-1. San Diego State Univ., Hubbs/Sea World Res. Inst., and USAF Space Div.

Carlson, H. W. & Maglieri, D. I. 1972 *J. Acoust Soc. Am.* **51**, 675–685.

Carrier, G. F., Krook, M. & Pearson, C. E. 1966 *Function of a Complex Variable*, pp. 252–276, 301–332. McGraw Hill.

Cheng, H. K., Kunc, J. & Edwards, J. R. 2003 Sonic boom excited sediment waves: a model study. *Canadian acoustics. J. Can. Acoust. Assoc.* **34** (4), 5–18.

Cheng, H. K. & Lee, C. J. 1997 Submarine impact of sonic booms: a study comparing and reconciling results from two prediction approaches. *Proc. Noise Conf. 97, Penn. State Univ., June 15–17, 1997* (ed. C. L. Burroughs), pp. 399–404.

Cheng, H. K. & Lee, C. J. 1998 A theory of sonic boom noise penetration under a wavy ocean. *AIAA Paper* 98-2958.

Cheng, H. K. & Lee, C. J. 2000 Sonic boom noise penetration under a wavy ocean: Part I. Theory. *Univ. So. Calif., USC AME Rep.* 11-11-2000 (available at www-rcf.usc.edu/hkcheng).

Cheng, H. K., Lee, C. J. & Edwards, J. R. 2001 Sonic boom noise penetration under a wavy ocean: Part II. Examples and extensions. *Univ. So. Calif., USC AME Rep* 4-4-2001.

Cook, R. 1970 *J. Acoust. Soc. Am.* **97**, 159–162.

Desharnais, F. & Chapman, D. M. F. 2002 *J. Acoustic Soc. Am.* **111**, 540–553.

D'Spain, G. L., Kuperman, W. A., Hodgkiss, W. S. & Berger, L. P. 1995 3-D localization of a blue whale. *Univ. Calif. Scripps Inst. Oceanography, Marine Phys. Lab. Tech. Memo.* 447, MPL-U-87/95.

Fincham, A. & Maxworthy, T. 2001 An experimental study of sonic boom penetration under a wavy air-water interface. *Univ. So. Calif. Aero.and Mech. Eng. USC AME Rep.* 09-11-2001.

Frankel, A. S. & Clark, C. W. 1998 *Can. J. Zool.* **76**, 521–535.

Greene, C. R. 1985 A pilot study of possible effects of marine seismic airgun array operation on rockfish plubmes. Report from Greenridge Science Inc., Santa Barbara, CA, for Seismic Steering Commetee, 50 p.

Hayes, W. D. 1971 *Annu. Rev. Fluid Mech.* **3**, 69–290.

Intrieri, P. E. & Malcolm, G. N. 1973 *AIAA J.* **11**, 510–516.

Landau, L. D. & Liftshitz, E. M. 1959 *Fluid Mechanics*, pp. 269–270. Pergaman.

Lighthill, M. J. 1964 *Fourier Analysis and Generalized Functions*, Table I, p. 43. Cambridge University Press.

Lighthill, M. J. 1978 *Waves in Fluids*, pp. 249, 250. Cambridge University Press.

Medwin, H., Helbig, R. A. & Hagy, J. D. Jr 1973 *J. Acoust. Soc. Am.* **54**, 99–109.

Miles, J. 1959 *Potential Theory of Unsteady Supersonic Flow*. Cambridge University Press.

Munk, W., Worchester, P. & Wunsch, C. 1995 *Ocean Acoustic Tomography*. Cambridge University Press.

NRC 1992 *Low-Frequency Sound and Marine Mammals*. National Res. Council Ocean Study Board Committee, p. viii.

NRDC 1999 *Sounding the Depth: Supertanker, Sonar, and the Rise of Undersea Noise*. National Resource Defense Council.

Pierce, A. D. 1991 *Acoustics*, pp. 75–82. Acoustic Soc. Am.

Richardson, W. J., Greene, C. R., Malme, C. I. & Thomson, D. H. 1995 *Marine Mammals and Noise*, pp. 15–86, 425–452. Academic.

Rochat, J. L. & Sparrow, V. W. 1997 *AIAA J.* **35**, 35–39.

Sawyers, K. H. 1968 *J. Acoust. Soc. Am.* **44**, 523–524.

Sohn, R. A., Vernon, F., Hildebrand, J. A. & Webb, S. C. 1999 *J. Acoust. Soc. Am.* **107**, 3073–3083.

Sparrow, V. W. 1995 *J. Acoust. Soc. Am.* **97**, 159–162.

Sparrow, V. W. & Ferguson, T. 1997 Penetration of a sharp sonic boom noise Into a flat ocean. *AIAA Paper* 97-0486.

Titchmarsh, E. C. 1937 *Theory of Fourier Integrals*. Oxford University Press.

Tolstoy, I. & Clay, C. S. 1987 *Ocean Acoustics: Theory and Experiment in Underwater Sound*, pp. 40–42, 76–84. Published for Acoust. Soc. Am. by Am. Inst. Physics.

Urick, R. J. 1983 *Principles of Underwater Sound*, 3rd Edn. McGraw Hill.

Van Dyke, M. D. 1975 *Perturbation Methods in Fluid Mechanics*, annotated edition, pp. 106–120. Parabolic Press.

Water, J. 1971 Penetration of sonic energy Into the ocean: An experimental simulation. *Proc. Noise Control Conf., Purdue Univ., July 11–16 1971*, pp. 554–557.

Wenz, G. M. 1962 *J. Acoust. Soc. Am.* **34**, 1936–1956.

Whitham, G. B. 1974 *Linear and Nonlinear Waves*. Wiley.